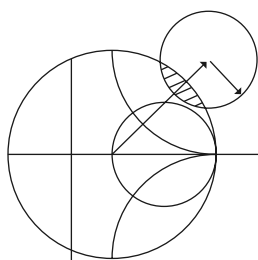


An abstract 3D graphic featuring a large, metallic-looking wheel with several spokes. The wheel is positioned on the right side of the cover, with its rim and spokes extending towards the center. The spokes are thick and curved, creating a sense of depth and movement. The background is a gradient of dark purple and blue, with the wheel's surface reflecting light, giving it a polished, metallic appearance. The overall composition is dynamic and modern, suggesting a focus on engineering and technology.

DAVID M. POZAR

MICROWAVE ENGINEERING

FOURTH EDITION



Microwave Network Analysis

Circuits operating at low frequencies, for which the circuit dimensions are small relative to the wavelength, can be treated as an interconnection of lumped passive or active components with unique voltages and currents defined at any point in the circuit. In this situation the circuit dimensions are small enough such that there is negligible phase delay from one point in the circuit to another. In addition, the fields can be considered as TEM fields supported by two or more conductors. This leads to a quasi-static type of solution to Maxwell's equations and to the well-known Kirchhoff voltage and current laws and impedance concepts of circuit theory [1]. As the reader is aware, there is a powerful and useful set of techniques for analyzing low-frequency circuits. In general, these techniques cannot be directly applied to microwave circuits, but it is the purpose of the present chapter to show how basic circuit and network concepts can be extended to handle many microwave analysis and design problems of practical interest.

The main reason for doing this is that it is usually much easier to apply the simple and intuitive ideas of circuit analysis to a microwave problem than it is to solve Maxwell's equations for the same problem. In a way, field analysis gives us much more information about the particular problem under consideration than we really want or need. That is, because the solution to Maxwell's equations for a given problem is complete, it gives the electric and magnetic fields at all points in space. However, usually we are only interested in the voltage or current at a set of terminals, the power flow through a device, or some other type of "terminal" quantity, as opposed to a minute description of the fields at all points in space. Another reason for using circuit or network analysis is that it is then very easy to modify the original problem, or combine several elements together and find the response, without having to reanalyze in detail the behavior of each element in combination with its neighbors. A field analysis using Maxwell's equations for such problems would be hopelessly difficult. There are situations, however, in which such circuit analysis techniques are an oversimplification and may lead to erroneous results. In such cases one must resort to a field analysis approach, using Maxwell's equations. Fortunately, there are a number of commercially available computer-aided design packages that can model RF and microwave problems using both field theory analysis and network analysis. It is part of the education of a microwave engineer to be able to determine when network analysis concepts apply and when they should be cast aside in favor of more rigorous analysis.

The basic procedure for microwave network analysis is as follows. We first treat a set of basic, canonical problems rigorously, using field analysis and Maxwell's equations (as we have done in Chapters 2 and 3, for a variety of transmission line and waveguide problems). When so doing, we try to obtain quantities that can be directly related to a circuit or transmission line parameter. For example, when we treated various transmission lines and waveguides in Chapter 3 we derived the propagation constant and characteristic impedance of the line. This allowed the transmission line or waveguide to be treated as an idealized distributed component characterized by its length, propagation constant, and characteristic impedance. At this point, we can interconnect various components and use network and/or transmission line theory to analyze the behavior of the entire system of components, including effects such as multiple reflections, loss, impedance transformations, and transitions from one type of transmission medium to another (e.g., coax to microstrip). As we will see, a transition between different transmission lines, or a discontinuity on a transmission line, generally cannot be treated as a simple junction between two transmission lines, but typically includes some type of equivalent circuit to account for reactances associated with the transition or discontinuity.

Microwave network theory was originally developed in the service of radar system and component development at the MIT Radiation Lab in the 1940s. This work was continued at the Polytechnic Institute of Brooklyn and other locations by researchers such as E. Weber, N. Marcuvitz, A. A. Oliner, L. B. Felsen, A. Hessel, and many others [2].

4.1

IMPEDANCE AND EQUIVALENT VOLTAGES AND CURRENTS

Equivalent Voltages and Currents

At microwave frequencies the measurement of voltage or current is difficult (or impossible), unless a clearly defined terminal pair is available. Such a terminal pair may be present in the case of TEM-type lines (such as coaxial cable, microstrip line, or stripline), but does not strictly exist for non-TEM lines (such as rectangular, circular, or surface waveguides).

Figure 4.1 shows the electric and magnetic field lines for an arbitrary two-conductor TEM transmission line. As in Chapter 3, the voltage, V , of the + conductor relative to the – conductor can be found as

$$V = \int_{+}^{-} \vec{E} \cdot d\vec{\ell}, \quad (4.1)$$

where the integration path begins on the + conductor and ends on the – conductor. It is important to realize that, because of the electrostatic nature of the transverse fields between the two conductors, the voltage defined in (4.1) is unique and does not depend on the shape of the integration path. The total current flowing on the + conductor can be determined from an application of Ampere's law as

$$I = \oint_{C^{+}} \vec{H} \cdot d\vec{\ell}, \quad (4.2)$$

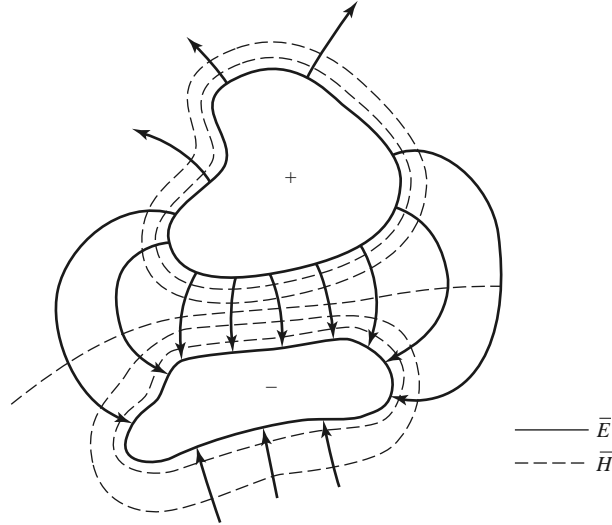


FIGURE 4.1 Electric and magnetic field lines for an arbitrary two-conductor TEM line.

where the integration contour is any closed path enclosing the + conductor (but not the - conductor). A characteristic impedance Z_0 can then be defined for traveling waves as

$$Z_0 = \frac{V}{I}. \quad (4.3)$$

At this point, after having defined and determined a voltage, current, and characteristic impedance (and assuming we know the propagation constant for the line), we can proceed to apply the circuit theory for transmission lines developed in Chapter 2 to characterize this line as a circuit element.

The situation is more difficult for waveguides. To see why, we will look at the case of a rectangular waveguide, as shown in Figure 4.2. For the dominant TE_{10} mode, the transverse fields can be written, from Table 3.2, as

$$E_y(x, y, z) = \frac{j\omega\mu a}{\pi} A \sin \frac{\pi x}{a} e^{-j\beta z} = A e_y(x, y) e^{-j\beta z}, \quad (4.4a)$$

$$H_x(x, y, z) = \frac{j\beta a}{\pi} A \sin \frac{\pi x}{a} e^{-j\beta z} = A h_x(x, y) e^{-j\beta z}. \quad (4.4b)$$

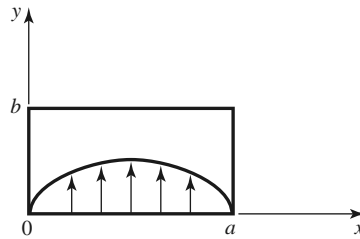


FIGURE 4.2 Electric field lines for the TE_{10} mode of a rectangular waveguide.

Applying (4.1) to the electric field of (4.4a) gives

$$V = \frac{-j\omega\mu a}{\pi} A \sin \frac{\pi x}{a} e^{-j\beta z} \int_y dy. \quad (4.5)$$

Thus it is seen that this voltage depends on the position, x , as well as the length of the integration contour along the y direction. For example, integrating from $y = 0$ to b for $x = a/2$ gives a voltage that is quite different from that obtained by integrating from $y = 0$ to b for $x = 0$. What, then, is the correct voltage? The answer is that there is no “correct” voltage in the sense of being unique or pertinent for all applications. A similar problem arises with current, and also impedance. We will now show how we can define *equivalent* voltages, currents, and impedances that can be useful for non-TEM lines.

There are many ways to define equivalent voltage, current, and impedance for waveguides since these quantities are not unique for non-TEM lines, but the following considerations usually lead to the most useful results [1, 3, 4]:

- Voltage and current are defined only for a particular waveguide mode, and are defined so that the voltage is proportional to the transverse electric field and the current is proportional to the transverse magnetic field.
- In order to be useful in a manner similar to voltages and currents of circuit theory, the equivalent voltages and currents should be defined so that their product gives the power flow of the waveguide mode.
- The ratio of the voltage to the current for a single traveling wave should be equal to the characteristic impedance of the line. This impedance may be chosen arbitrarily, but is usually selected as equal to the wave impedance of the line, or else normalized to unity.

For an arbitrary waveguide mode with both positively and negatively traveling waves, the transverse fields can be written as

$$\bar{E}_t(x, y, z) = \bar{e}(x, y)(A^+ e^{-j\beta z} + A^- e^{j\beta z}) = \frac{\bar{e}(x, y)}{C_1}(V^+ e^{-j\beta z} + V^- e^{j\beta z}), \quad (4.6a)$$

$$\bar{H}_t(x, y, z) = \bar{h}(x, y)(A^+ e^{-j\beta z} - A^- e^{j\beta z}) = \frac{\bar{h}(x, y)}{C_2}(I^+ e^{-j\beta z} - I^- e^{j\beta z}), \quad (4.6b)$$

where \bar{e} and \bar{h} are the transverse field variations of the mode, and A^+ , A^- are the field amplitudes of the traveling waves. Because \bar{E}_t and \bar{H}_t are related by the wave impedance, Z_w , according to (3.22) or (3.26), we also have that

$$\bar{h}(x, y) = \frac{\hat{z} \times \bar{e}(x, y)}{Z_w}. \quad (4.7)$$

Equation (4.6) also defines equivalent voltage and current waves as

$$V(z) = V^+ e^{-j\beta z} + V^- e^{j\beta z}, \quad (4.8a)$$

$$I(z) = I^+ e^{-j\beta z} - I^- e^{j\beta z}, \quad (4.8b)$$

with $V^+/I^+ = V^-/I^- = Z_0$. This definition embodies the idea of making the equivalent voltage and current proportional to the transverse electric and magnetic fields, respectively. The proportionality constants for this relationship are $C_1 = V^+/A^+ = V^-/A^-$ and $C_2 = I^+/A^+ = I^-/A^-$, and can be determined from the remaining two conditions for power and impedance.

The complex power flow for the incident wave is given by

$$P^+ = \frac{1}{2} |A^+|^2 \int_S \bar{\mathbf{e}} \times \bar{\mathbf{h}}^* \cdot \hat{\mathbf{z}} ds = \frac{V^+ I^{+*}}{2C_1 C_2^*} \int_S \bar{\mathbf{e}} \times \bar{\mathbf{h}}^* \cdot \hat{\mathbf{z}} ds. \quad (4.9)$$

Because we want this power to be equal to $(1/2)V^+ I^{+*}$, we have the result that

$$C_1 C_2^* = \int_S \bar{\mathbf{e}} \times \bar{\mathbf{h}}^* \cdot \hat{\mathbf{z}} ds, \quad (4.10)$$

where the surface integration is over the cross section of the waveguide. The characteristic impedance is

$$Z_0 = \frac{V^+}{I^+} = \frac{V^-}{I^-} = \frac{C_1}{C_2}, \quad (4.11)$$

since $V^+ = C_1 A$ and $I^+ = C_2 A$, from (4.6a) and (4.6b). If it is desired to have $Z_0 = Z_w$, the wave impedance (Z_{TE} or Z_{TM}) of the mode, then

$$\frac{C_1}{C_2} = Z_w (Z_{TE} \text{ or } Z_{TM}). \quad (4.12a)$$

Alternatively, it may be desirable to normalize the characteristic impedance to unity ($Z_0 = 1$), in which case we have

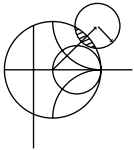
$$\frac{C_1}{C_2} = 1. \quad (4.12b)$$

For a given waveguide mode, (4.10) and (4.12) can be solved for the constants C_1 and C_2 , and equivalent voltages and currents defined. Higher order modes can be treated in the same way, so that a general field in a waveguide can be expressed in the following form:

$$\bar{\mathbf{E}}_t(x, y, z) = \sum_{n=1}^N \left(\frac{V_n^+}{C_{1n}} e^{-j\beta_n z} + \frac{V_n^-}{C_{1n}} e^{j\beta_n z} \right) \bar{\mathbf{e}}_n(x, y), \quad (4.13a)$$

$$\bar{\mathbf{H}}_t(x, y, z) = \sum_{n=1}^N \left(\frac{I_n^+}{C_{2n}} e^{-j\beta_n z} - \frac{I_n^-}{C_{2n}} e^{j\beta_n z} \right) \bar{\mathbf{h}}_n(x, y), \quad (4.13b)$$

where V_n^\pm and I_n^\pm are the equivalent voltages and currents for the n th mode, and C_{1n} and C_{2n} are the proportionality constants for each mode.



EXAMPLE 4.1 EQUIVALENT VOLTAGE AND CURRENT FOR A RECTANGULAR WAVEGUIDE

Find the equivalent voltages and currents for a TE_{10} mode in a rectangular waveguide.

Solution

The transverse field components and power flow of the TE_{10} rectangular waveguide mode and the equivalent transmission line model of this mode can be written as follows:

| Waveguide Fields | Transmission Line Model |
|---|---|
| $E_y = (A^+ e^{-j\beta z} + A^- e^{j\beta z}) \sin \frac{\pi x}{a}$ | $V(z) = V^+ e^{-j\beta z} + V^- e^{j\beta z}$ |
| $H_x = \frac{-1}{Z_{TE}} (A^+ e^{-j\beta z} - A^- e^{j\beta z}) \sin \frac{\pi x}{a}$ | $I(z) = I^+ e^{-j\beta z} - I^- e^{j\beta z}$ $= \frac{1}{Z_0} (V^+ e^{-j\beta z} - V^- e^{j\beta z})$ |
| $P^+ = \frac{-1}{2} \int_S E_y H_x^* dx dy = \frac{ab}{4Z_{TE}} A^+ ^2$ | $P^+ = \frac{1}{2} V^+ I^{+*}$ |

We now find the constants $C_1 = V^+/A^+ = V^-/A^-$ and $C_2 = I^+/A^+ = I^-/A^-$ that relate the equivalent voltages V^\pm and currents I^\pm to the field amplitudes, A^\pm . Equating incident powers gives

$$\frac{ab |A^+|^2}{4Z_{TE}} = \frac{1}{2} V^+ I^{+*} = \frac{1}{2} |A^+|^2 C_1 C_2^*.$$

If we choose $Z_0 = Z_{TE}$, then we also have that

$$\frac{V^+}{I^+} = \frac{C_1}{C_2} = Z_{TE}.$$

Solving for C_1 , C_2 gives

$$C_1 = \sqrt{\frac{ab}{2}},$$

$$C_2 = \frac{1}{Z_{TE}} \sqrt{\frac{ab}{2}},$$

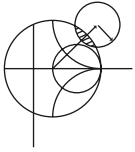
which completes the transmission line equivalence for the TE_{10} mode. ■

The Concept of Impedance

We have used the idea of impedance in several different ways, so it may be useful at this point to summarize this important concept. The term *impedance* was first used by Oliver Heaviside in the nineteenth century to describe the complex ratio V/I in AC circuits consisting of resistors, inductors, and capacitors; the impedance concept quickly became indispensable in the analysis of AC circuits. It was then applied to transmission lines, in terms of lumped-element equivalent circuits and the distributed series impedance and shunt admittance of the line. In the 1930s, S. A. Schelkunoff recognized that the impedance concept could be extended to electromagnetic fields in a systematic way, and noted that impedance should be regarded as characteristic of the type of field, as well as of the medium [2]. In addition, in relation to the analogy between transmission lines and plane wave propagation, impedance may even be dependent on direction. The concept of impedance, then, forms an important link between field theory and transmission line or circuit theory.

We summarize the various types of impedance we have used so far, and their notation:

- $\eta = \sqrt{\mu/\epsilon} =$ intrinsic impedance of the medium. This impedance is dependent only on the material parameters of the medium, and is equal to the wave impedance for plane waves.
- $Z_w = E_t/H_t = 1/Y_w =$ wave impedance. This impedance is a characteristic of the particular type of wave. TEM, TM, and TE waves each have different wave impedances (Z_{TEM} , Z_{TM} , Z_{TE}), which may depend on the type of line or guide, the material, and the operating frequency.
- $Z_0 = 1/Y_0 = V^+/I^+ =$ characteristic impedance. Characteristic impedance is the ratio of voltage to current for a traveling wave on a transmission line. Because voltage and current are uniquely defined for TEM waves, the characteristic impedance of a TEM wave is unique. TE and TM waves, however, do not have a uniquely defined voltage and current, so the characteristic impedance for such waves may be defined in different ways.



EXAMPLE 4.2 APPLICATION OF WAVEGUIDE IMPEDANCE

Consider a rectangular waveguide with $a = 2.286$ cm and $b = 1.016$ cm (X-band guide), air filled for $z < 0$ and Rexolite filled ($\epsilon_r = 2.54$) for $z > 0$, as shown in Figure 4.3. If the operating frequency is 10 GHz, use an equivalent transmission line model to compute the reflection coefficient of a TE_{10} wave incident on the interface from $z < 0$.

Solution

The waveguide propagation constants in the air ($z < 0$) and the dielectric ($z > 0$) regions are

$$\beta_a = \sqrt{k_0^2 - \left(\frac{\pi}{a}\right)^2} = 158.0 \text{ m}^{-1},$$

$$\beta_d = \sqrt{\epsilon_r k_0^2 - \left(\frac{\pi}{a}\right)^2} = 304.1 \text{ m}^{-1},$$

where $k_0 = 209.4 \text{ m}^{-1}$.

The reader may verify that the TE_{10} mode is the only propagating mode in either waveguide region. We can set up an equivalent transmission line for the TE_{10} mode in each waveguide, and treat the problem as the reflection of an incident voltage wave at the junction of two infinite transmission lines.

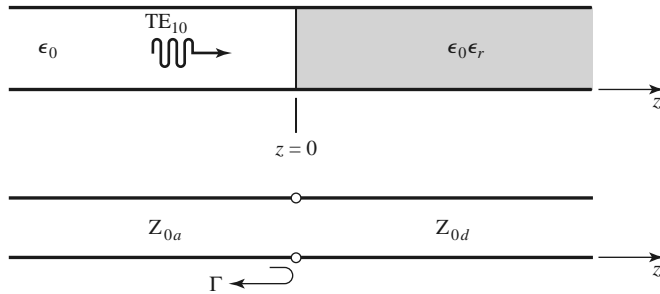


FIGURE 4.3 Geometry of a partially filled waveguide and its transmission line equivalent for Example 4.2.

By Example 4.1 and Table 3.2, the equivalent characteristic impedances for the two lines are

$$Z_{0a} = \frac{k_0 \eta_0}{\beta_a} = \frac{(209.4)(377)}{158.0} = 500.0 \, \Omega,$$

$$Z_{0d} = \frac{k\eta}{\beta_d} = \frac{k_0 \eta_0}{\beta_d} = \frac{(209.4)(377)}{304.1} = 259.6 \, \Omega.$$

The reflection coefficient seen looking into the dielectric filled region is then

$$\Gamma = \frac{Z_{0d} - Z_{0a}}{Z_{0d} + Z_{0a}} = -0.316.$$

With this result, expressions for the incident, reflected, and transmitted waves can be written in terms of fields, or in terms of equivalent voltages and currents. ■

We now consider the arbitrary one-port network shown in Figure 4.4 and derive a general relation between its impedance properties and electromagnetic energy stored in, and the power dissipated by, the network. The complex power delivered to this network is given by (1.91):

$$P = \frac{1}{2} \oint_S \bar{\mathbf{E}} \times \bar{\mathbf{H}}^* \cdot d\bar{\mathbf{s}} = P_\ell + 2j\omega(W_m - W_e), \quad (4.14)$$

where P_ℓ is real and represents the average power dissipated by the network, and W_m and W_e represent the stored magnetic and electric energy, respectively. Note that the unit normal vector in Figure 4.4 is pointing into the volume.

If we define real transverse modal fields $\bar{\mathbf{e}}$ and $\bar{\mathbf{h}}$ over the terminal plane of the network such that

$$\bar{\mathbf{E}}_t(x, y, z) = V(z)\bar{\mathbf{e}}(x, y)e^{-j\beta z}, \quad (4.15a)$$

$$\bar{\mathbf{H}}_t(x, y, z) = I(z)\bar{\mathbf{h}}(x, y)e^{-j\beta z}, \quad (4.15b)$$

with a normalization such that

$$\int_S \bar{\mathbf{e}} \times \bar{\mathbf{h}} \cdot d\bar{\mathbf{s}} = 1,$$

then we can express (4.14) in terms of the terminal voltage and current:

$$P = \frac{1}{2} \int_S V\Gamma^* \bar{\mathbf{e}} \times \bar{\mathbf{h}} \cdot d\bar{\mathbf{s}} = \frac{1}{2} V\Gamma^*. \quad (4.16)$$

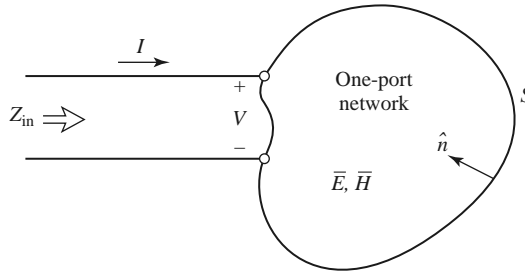


FIGURE 4.4 An arbitrary one-port network.

Then the input impedance is

$$Z_{\text{in}} = R + jX = \frac{V}{I} = \frac{VI^*}{|I|^2} = \frac{P}{\frac{1}{2}|I|^2} = \frac{P_\ell + 2j\omega(W_m - W_e)}{\frac{1}{2}|I|^2}. \quad (4.17)$$

Thus we see that the real part, R , of the input impedance is related to the dissipated power, while the imaginary part, X , is related to the net energy stored in the network. If the network is lossless, then $P_\ell = 0$ and $R = 0$. Then Z_{in} is purely imaginary, with a reactance

$$X = \frac{4\omega(W_m - W_e)}{|I|^2}, \quad (4.18)$$

which is positive for an inductive load ($W_m > W_e$), and negative for a capacitive load ($W_m < W_e$).

Even and Odd Properties of $Z(\omega)$ and $\Gamma(\omega)$

Consider the driving point impedance, $Z(\omega)$, at the input port of an electrical network. The voltage and current at this port are related as $V(\omega) = Z(\omega)I(\omega)$. For an arbitrary frequency dependence, we can find the time-domain voltage by taking the inverse Fourier transform of $V(\omega)$:

$$v(t) = \frac{1}{2\pi} \int_{-\infty}^{\infty} V(\omega)e^{j\omega t} d\omega. \quad (4.19)$$

Because $v(t)$ must be real, we have that $v(t) = v^*(t)$, or

$$\int_{-\infty}^{\infty} V(\omega)e^{j\omega t} d\omega = \int_{-\infty}^{\infty} V^*(\omega)e^{-j\omega t} d\omega = \int_{-\infty}^{\infty} V^*(-\omega)e^{j\omega t} d\omega,$$

where the last term was obtained by a change of variable from ω to $-\omega$. This shows that $V(\omega)$ must satisfy the relation

$$V(-\omega) = V^*(\omega), \quad (4.20)$$

which means that $\text{Re}\{V(\omega)\}$ is even in ω , while $\text{Im}\{V(\omega)\}$ is odd in ω . Similar results hold for $I(\omega)$, and for $Z(\omega)$ since

$$V^*(-\omega) = Z^*(-\omega)I^*(-\omega) = Z^*(-\omega)I(\omega) = V(\omega) = Z(\omega)I(\omega).$$

Thus, if $Z(\omega) = R(\omega) + jX(\omega)$, then $R(\omega)$ is even in ω and $X(\omega)$ is odd in ω . These results can also be inferred from (4.17).

Now consider the reflection coefficient at the input port:

$$\Gamma(\omega) = \frac{Z(\omega) - Z_0}{Z(\omega) + Z_0} = \frac{R(\omega) - Z_0 + jX(\omega)}{R(\omega) + Z_0 + jX(\omega)}. \quad (4.21)$$

Then

$$\Gamma(-\omega) = \frac{R(\omega) - Z_0 - jX(\omega)}{R(\omega) + Z_0 - jX(\omega)} = \Gamma^*(\omega), \quad (4.22)$$

which shows that the real and imaginary parts of $\Gamma(\omega)$ are even and odd, respectively, in ω . Finally, the magnitude of the reflection coefficient is

$$|\Gamma(\omega)|^2 = \Gamma(\omega)\Gamma^*(\omega) = \Gamma(\omega)\Gamma(-\omega) = |\Gamma(-\omega)|^2, \quad (4.23)$$

which shows that $|\Gamma(\omega)|^2$ and $|\Gamma(\omega)|$ are even functions of ω . This result implies that only even series of the form $a + b\omega^2 + c\omega^4 + \dots$ can be used to represent $|\Gamma(\omega)|$ or $|\Gamma(\omega)|^2$.

4.2

IMPEDANCE AND ADMITTANCE MATRICES

In the previous section we have seen how equivalent voltages and currents can be defined for TEM and non-TEM waves. Once such voltages and currents have been defined at various points in a microwave network, we can use the impedance and/or admittance matrices of circuit theory to relate these terminal or *port* quantities to each other, and thus to essentially arrive at a matrix description of the network. This type of representation lends itself to the development of equivalent circuits of arbitrary networks, which will be quite useful when we discuss the design of passive components such as couplers and filters. (The term *port* was introduced by H. A. Wheeler in the 1950s to replace the less descriptive and more cumbersome phrase “two-terminal pair” [2, 3].)

We begin by considering an arbitrary N -port microwave network, as depicted in Figure 4.5. The ports in Figure 4.5 may be any type of transmission line or transmission line equivalent of a single propagating waveguide mode. If one of the physical ports of the network is a waveguide supporting more than one propagating mode, additional electrical ports can be added to account for these modes. At a specific point on the n th port, a terminal plane, t_n , is defined along with equivalent voltages and currents for the incident (V_n^+ , I_n^+) and reflected (V_n^- , I_n^-) waves. The terminal planes are important in providing a phase reference for the voltage and current phasors. Now, at the n th terminal plane, the total voltage and current are given by

$$V_n = V_n^+ + V_n^-, \quad (4.24a)$$

$$I_n = I_n^+ - I_n^-, \quad (4.24b)$$

as seen from (4.8) when $z = 0$.

The impedance matrix $[Z]$ of the microwave network then relates these voltages and currents:

$$\begin{bmatrix} V_1 \\ V_2 \\ \vdots \\ V_N \end{bmatrix} = \begin{bmatrix} Z_{11} & Z_{12} & \cdots & Z_{1N} \\ Z_{21} & & & \vdots \\ \vdots & & & \vdots \\ Z_{N1} & \cdots & \cdots & Z_{NN} \end{bmatrix} \begin{bmatrix} I_1 \\ I_2 \\ \vdots \\ I_N \end{bmatrix},$$

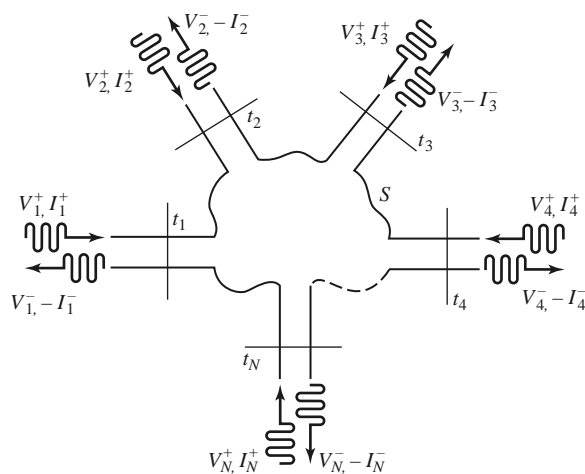


FIGURE 4.5 An arbitrary N -port microwave network.

or in matrix form as

$$[V] = [Z][I]. \quad (4.25)$$

Similarly, we can define an admittance matrix $[Y]$ as

$$\begin{bmatrix} I_1 \\ I_2 \\ \vdots \\ I_N \end{bmatrix} = \begin{bmatrix} Y_{11} & Y_{12} & \cdots & Y_{1N} \\ Y_{21} & & & \vdots \\ \vdots & & & \vdots \\ Y_{N1} & \cdots & \cdots & Y_{NN} \end{bmatrix} \begin{bmatrix} V_1 \\ V_2 \\ \vdots \\ V_N \end{bmatrix},$$

or in matrix form as

$$[I] = [Y][V]. \quad (4.26)$$

Of course, the $[Z]$ and $[Y]$ matrices are the inverses of each other:

$$[Y] = [Z]^{-1}. \quad (4.27)$$

Note that both the $[Z]$ and $[Y]$ matrices relate the total port voltages and currents.

From (4.25), we see that Z_{ij} can be found as

$$Z_{ij} = \left. \frac{V_i}{I_j} \right|_{I_k=0 \text{ for } k \neq j}. \quad (4.28)$$

In words, (4.28) states that Z_{ij} can be found by driving port j with the current I_j , open-circuiting all other ports (so $I_k = 0$ for $k \neq j$), and measuring the open-circuit voltage at port i . Thus, Z_{ii} is the input impedance seen looking into port i when all other ports are open-circuited, and Z_{ij} is the transfer impedance between ports i and j when all other ports are open-circuited.

Similarly, from (4.26), Y_{ij} can be found as

$$Y_{ij} = \left. \frac{I_i}{V_j} \right|_{V_k=0 \text{ for } k \neq j}, \quad (4.29)$$

which states that Y_{ij} can be determined by driving port j with the voltage V_j , short-circuiting all other ports (so $V_k = 0$ for $k \neq j$), and measuring the short-circuit current at port i .

In general, each Z_{ij} or Y_{ij} element may be complex. For an arbitrary N -port network, the impedance and admittance matrices are $N \times N$ in size, so there are $2N^2$ independent quantities or degrees of freedom. In practice, however, many networks are either reciprocal or lossless, or both. If the network is reciprocal (not containing any active devices or nonreciprocal media, such as ferrites or plasmas), we will show that the impedance and admittance matrices are symmetric, so that $Z_{ij} = Z_{ji}$, and $Y_{ij} = Y_{ji}$. If the network is lossless, we can show that all the Z_{ij} or Y_{ij} elements are purely imaginary. Either of these special cases serves to reduce the number of independent quantities or degrees of freedom that an N -port network may have. We now derive the above characteristics for reciprocal and lossless networks.

Reciprocal Networks

Consider the arbitrary network of Figure 4.5 to be reciprocal (no active devices, ferrites, or plasmas), with short circuits placed at all terminal planes except those of ports 1 and 2. Let \bar{E}_a , \bar{H}_a and \bar{E}_b , \bar{H}_b be the fields anywhere in the network due to two independent sources,

a and b , located somewhere in the network. Then the reciprocity theorem of (1.156) states that

$$\oint_S \bar{E}_a \times \bar{H}_b \cdot d\bar{s} = \oint_S \bar{E}_b \times \bar{H}_a \cdot d\bar{s}, \quad (4.30)$$

where S is the closed surface along the boundaries of the network and through the terminal planes of the ports. If the boundary walls of the network and transmission lines are metal, then $\bar{E}_{\text{tan}} = 0$ on these walls (assuming perfect conductors). If the network or the transmission lines are open structures, like microstrip line or slotline, the boundaries of the network can be taken arbitrarily far from the lines so that \bar{E}_{tan} is negligible. Then the only nonzero contribution to the integrals of (4.30) come from the cross-sectional areas of ports 1 and 2.

From Section 4.1, the fields due to sources a and b can be evaluated at the terminal planes t_1 and t_2 as

$$\bar{E}_{1a} = V_{1a}\bar{e}_1, \quad \bar{H}_{1a} = I_{1a}\bar{h}_1, \quad (4.31a)$$

$$\bar{E}_{1b} = V_{1b}\bar{e}_1, \quad \bar{H}_{1b} = I_{1b}\bar{h}_1, \quad (4.31b)$$

$$\bar{E}_{2a} = V_{2a}\bar{e}_2, \quad \bar{H}_{2a} = I_{2a}\bar{h}_2, \quad (4.31c)$$

$$\bar{E}_{2b} = V_{2b}\bar{e}_2, \quad \bar{H}_{2b} = I_{2b}\bar{h}_2, \quad (4.31d)$$

where \bar{e}_1 , \bar{h}_1 and \bar{e}_2 , \bar{h}_2 are the transverse modal fields of ports 1 and 2, respectively, and the V s and I s are the equivalent total voltages and currents. (For instance, \bar{E}_{1b} is the transverse electric field at terminal plane t_1 of port 1 due to source b .) Substituting the fields of (4.31) into (4.30) gives

$$(V_{1a}I_{1b} - V_{1b}I_{1a}) \int_{S_1} \bar{e}_1 \times \bar{h}_1 \cdot d\bar{s} + (V_{2a}I_{2b} - V_{2b}I_{2a}) \int_{S_2} \bar{e}_2 \times \bar{h}_2 \cdot d\bar{s} = 0, \quad (4.32)$$

where S_1 and S_2 are the cross-sectional areas at the terminal planes of ports 1 and 2.

As in Section 4.1, the equivalent voltages and currents have been defined so that the power through a given port can be expressed as $VI^*/2$; then, comparing (4.31) to (4.6) implies that $C_1 = C_2 = 1$ for each port, so that

$$\int_{S_1} \bar{e}_1 \times \bar{h}_1 \cdot d\bar{s} = \int_{S_2} \bar{e}_2 \times \bar{h}_2 \cdot d\bar{s} = 1. \quad (4.33)$$

This reduces (4.32) to

$$V_{1a}I_{1b} - V_{1b}I_{1a} + V_{2a}I_{2b} - V_{2b}I_{2a} = 0. \quad (4.34)$$

Now use the 2×2 admittance matrix of the (effectively) two-port network to eliminate the I s:

$$I_1 = Y_{11}V_1 + Y_{12}V_2,$$

$$I_2 = Y_{21}V_1 + Y_{22}V_2.$$

Substitution into (4.34) gives

$$(V_{1a}V_{2b} - V_{1b}V_{2a})(Y_{12} - Y_{21}) = 0. \quad (4.35)$$

Because the sources a and b are independent, the voltages V_{1a} , V_{1b} , V_{2a} , and V_{2b} can take on arbitrary values. So in order for (4.35) to be satisfied for any choice of sources, we must have $Y_{12} = Y_{21}$, and since the choice of which ports are labeled as 1 and 2 is arbitrary, we have the general result that

$$Y_{ij} = Y_{ji}. \quad (4.36)$$

Then if $[Y]$ is a symmetric matrix, its inverse, $[Z]$, is also symmetric.

Lossless Networks

Now consider a reciprocal lossless N -port junction; we will show that the elements of the impedance and admittance matrices must be pure imaginary. If the network is lossless, then the net real power delivered to the network must be zero. Thus, $\text{Re}\{P_{\text{avg}}\} = 0$, where

$$\begin{aligned} P_{\text{avg}} &= \frac{1}{2}[V]^t[I]^* = \frac{1}{2}([Z][I])^t[I]^* = \frac{1}{2}[I]^t[Z][I]^* \\ &= \frac{1}{2}(I_1 Z_{11} I_1^* + I_1 Z_{12} I_2^* + I_2 Z_{21} I_1^* + \cdots) \\ &= \frac{1}{2} \sum_{n=1}^N \sum_{m=1}^N I_m Z_{mn} I_n^*. \end{aligned} \quad (4.37)$$

We have used the result from matrix algebra that $([A][B])^t = [B]^t[A]^t$. Because the I_n are independent, we must have the real part of each self term ($I_n Z_{nn} I_n^*$) equal to zero, since we could set all port currents equal to zero except for the n th current. So,

$$\text{Re}\{I_n Z_{nn} I_n^*\} = |I_n|^2 \text{Re}\{Z_{nn}\} = 0,$$

or

$$\text{Re}\{Z_{nn}\} = 0. \quad (4.38)$$

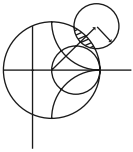
Now let all port currents be zero except for I_m and I_n . Then (4.37) reduces to

$$\text{Re}\{(I_n I_m^* + I_m I_n^*) Z_{mn}\} = 0,$$

since $Z_{mn} = Z_{nm}$. However, $(I_n I_m^* + I_m I_n^*)$ is a purely real quantity that is, in general, nonzero. Thus we must have that

$$\text{Re}\{Z_{mn}\} = 0. \quad (4.39)$$

Then (4.38) and (4.39) imply that $\text{Re}\{Z_{mn}\} = 0$ for any m, n . The reader can verify that this also leads to an imaginary $[Y]$ matrix.



EXAMPLE 4.3 EVALUATION OF IMPEDANCE PARAMETERS

Find the Z parameters of the two-port T-network shown in Figure 4.6.

Solution

From (4.28), Z_{11} can be found as the input impedance of port 1 when port 2 is open-circuited:

$$Z_{11} = \left. \frac{V_1}{I_1} \right|_{I_2=0} = Z_A + Z_C.$$

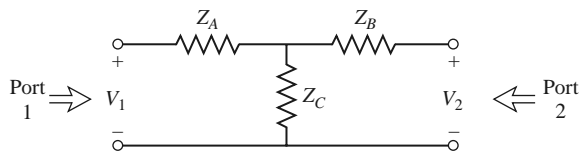


FIGURE 4.6 A two-port T-network.

The transfer impedance Z_{12} can be found measuring the open-circuit voltage at port 1 when a current I_2 is applied at port 2. By voltage division,

$$Z_{12} = \frac{V_1}{I_2} \Big|_{I_1=0} = \frac{V_2}{I_2} \frac{Z_C}{Z_B + Z_C} = Z_C.$$

The reader can verify that $Z_{21} = Z_{12}$, indicating that the circuit is reciprocal. Finally, Z_{22} is found as

$$Z_{22} = \frac{V_2}{I_2} \Big|_{I_1=0} = Z_B + Z_C. \quad \blacksquare$$

4.3

THE SCATTERING MATRIX

We have already discussed the difficulty in defining voltages and currents for non-TEM lines. In addition, a practical problem exists when trying to measure voltages and currents at microwave frequencies because direct measurements usually involve the magnitude (inferred from power) and phase of a wave traveling in a given direction or of a standing wave. Thus, equivalent voltages and currents, and the related impedance and admittance matrices, become somewhat of an abstraction when dealing with high-frequency networks. A representation more in accord with direct measurements, and with the ideas of incident, reflected, and transmitted waves, is given by the scattering matrix.

Like the impedance or admittance matrix for an N -port network, the scattering matrix provides a complete description of the network as seen at its N ports. While the impedance and admittance matrices relate the total voltages and currents at the ports, the scattering matrix relates the voltage waves incident on the ports to those reflected from the ports. For some components and circuits, the scattering parameters can be calculated using network analysis techniques. Otherwise, the scattering parameters can be measured directly with a vector network analyzer; a photograph of a modern network analyzer is shown in Figure 4.7. Once the scattering parameters of the network are known, conversion to other matrix parameters can be performed, if needed.

Consider the N -port network shown in Figure 4.5, where V_n^+ is the amplitude of the voltage wave incident on port n and V_n^- is the amplitude of the voltage wave reflected from port n . The scattering matrix, or $[S]$ matrix, is defined in relation to these incident and reflected voltage waves as

$$\begin{bmatrix} V_1^- \\ V_2^- \\ \vdots \\ V_N^- \end{bmatrix} = \begin{bmatrix} S_{11} & S_{12} & \cdots & S_{1N} \\ S_{21} & & & \vdots \\ S_{N1} & \cdots & & S_{NN} \\ \vdots & & & \end{bmatrix} \begin{bmatrix} V_1^+ \\ V_2^+ \\ \vdots \\ V_N^+ \end{bmatrix},$$

or

$$[V^-] = [S][V^+]. \quad (4.40)$$

A specific element of the scattering matrix can be determined as

$$S_{ij} = \frac{V_i^-}{V_j^+} \Big|_{V_k^+ = 0 \text{ for } k \neq j}. \quad (4.41)$$

In words, (4.41) says that S_{ij} is found by driving port j with an incident wave of voltage V_j^+ and measuring the reflected wave amplitude V_i^- coming out of port i . The incident

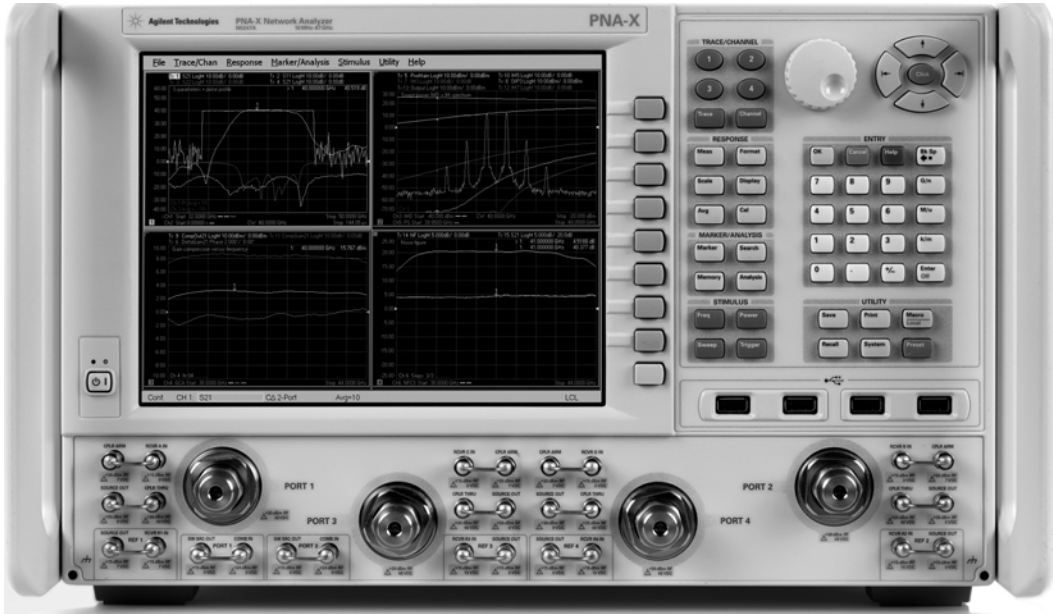
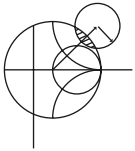


FIGURE 4.7 Photograph of the Agilent N5247A Programmable Network Analyzer. This instrument is used to measure the scattering parameters of RF and microwave networks from 10 MHz to 67 GHz. The instrument is programmable, performs error correction, and has a wide variety of display formats and data conversions.
Courtesy of Agilent Technologies.

waves on all ports except the j th port are set to zero, which means that all ports should be terminated in matched loads to avoid reflections. Thus, S_{ii} is the reflection coefficient seen looking into port i when all other ports are terminated in matched loads, and S_{ij} is the transmission coefficient from port j to port i when all other ports are terminated in matched loads.



EXAMPLE 4.4 EVALUATION OF SCATTERING PARAMETERS

Find the scattering parameters of the 3 dB attenuator circuit shown in Figure 4.8.

Solution

From (4.41), S_{11} can be found as the reflection coefficient seen at port 1 when port 2 is terminated in a matched load ($Z_0 = 50 \Omega$):

$$S_{11} = \left. \frac{V_1^-}{V_1^+} \right|_{V_2^+=0} = \Gamma^{(1)}|_{V_2^+=0} = \frac{Z_{\text{in}}^{(1)} - Z_0}{Z_{\text{in}}^{(1)} + Z_0} \bigg|_{Z_0 \text{ on port 2}},$$

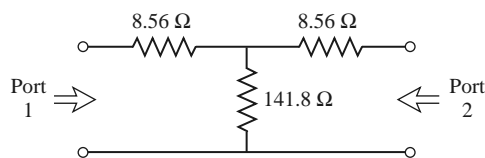


FIGURE 4.8 A matched 3 dB attenuator with a 50Ω characteristic impedance (Example 4.4).

but $Z_{\text{in}}^{(1)} = 8.56 + [141.8(8.56 + 50)]/(141.8 + 8.56 + 50) = 50 \Omega$, so $S_{11} = 0$. Because of the symmetry of the circuit, $S_{22} = 0$.

We can find S_{21} by applying an incident wave at port 1, V_1^+ , and measuring the outgoing wave at port 2, V_2^- . This is equivalent to the transmission coefficient from port 1 to port 2:

$$S_{21} = \left. \frac{V_2^-}{V_1^+} \right|_{V_2^+ = 0}.$$

From the fact that $S_{11} = S_{22} = 0$, we know that $V_1^- = 0$ when port 2 is terminated in $Z_0 = 50 \Omega$, and that $V_2^+ = 0$. In this case we have that $V_1^+ = V_1$ and $V_2^- = V_2$. By applying a voltage V_1 at port 1 and using voltage division twice we find $V_2^- = V_2$ as the voltage across the 50Ω load resistor at port 2:

$$V_2^- = V_2 = V_1 \left(\frac{41.44}{41.44 + 8.56} \right) \left(\frac{50}{50 + 8.56} \right) = 0.707 V_1,$$

where $41.44 = 141.8(58.56)/(141.8 + 58.56)$ is the resistance of the parallel combination of the 50Ω load and the 8.56Ω resistor with the 141.8Ω resistor. Thus, $S_{12} = S_{21} = 0.707$.

If the input power is $|V_1^+|^2/2Z_0$, then the output power is $|V_2^-|^2/2Z_0 = |S_{21}V_1^+|^2/2Z_0 = |S_{21}|^2/2Z_0|V_1^+|^2 = |V_1^+|^2/4Z_0$, which is one-half (-3 dB) of the input power. ■

We now show how the scattering matrix can be determined from the $[Z]$ (or $[Y]$) matrix and vice versa. First, we must assume that the characteristic impedances, Z_{0n} , of all the ports are identical. (This restriction will be removed when we discuss generalized scattering parameters.) Then, for convenience, we can set $Z_{0n} = 1$. From (4.24) the total voltage and current at the n th port can be written as

$$V_n = V_n^+ + V_n^-, \quad (4.42a)$$

$$I_n = I_n^+ - I_n^- = V_n^+ - V_n^-. \quad (4.42b)$$

Using the definition of $[Z]$ from (4.25) with (4.42) gives

$$[Z][I] = [Z][V^+] - [Z][V^-] = [V] = [V^+] + [V^-],$$

which can be rewritten as

$$([Z] + [U])[V^-] = ([Z] - [U])[V^+], \quad (4.43)$$

where $[U]$ is the unit, or identity, matrix defined as

$$[U] = \begin{bmatrix} 1 & 0 & \cdots & 0 \\ 0 & 1 & & \vdots \\ \vdots & & \ddots & \\ 0 & & \cdots & 1 \end{bmatrix}.$$

Comparing (4.43) to (4.40) suggests that

$$[S] = ([Z] + [U])^{-1} ([Z] - [U]), \quad (4.44)$$

giving the scattering matrix in terms of the impedance matrix. Note that for a one-port network (4.44) reduces to

$$S_{11} = \frac{z_{11} - 1}{z_{11} + 1},$$

in agreement with the result for the reflection coefficient seen looking into a load with a normalized input impedance of z_{11} .

To find $[Z]$ in terms of $[S]$, rewrite (4.44) as $[Z][S] + [U][S] = [Z] - [U]$, and solve for $[Z]$ to give

$$[Z] = ([U] + [S]) ([U] - [S])^{-1}. \quad (4.45)$$

Reciprocal Networks and Lossless Networks

As we discussed in Section 4.2, the impedance and admittance matrices are symmetric for reciprocal networks, and are purely imaginary for lossless networks. The scattering matrices for these particular types of networks also have special properties. We will show that the scattering matrix for a reciprocal network is symmetric, and that the scattering matrix for a lossless network is unitary.

By adding (4.42a) and (4.42b) we obtain

$$V_n^+ = \frac{1}{2}(V_n + I_n),$$

or

$$[V^+] = \frac{1}{2}([Z] + [U])[I]. \quad (4.46a)$$

By subtracting (4.42a) and (4.42b) we obtain

$$V_n^- = \frac{1}{2}(V_n - I_n),$$

or

$$[V^-] = \frac{1}{2}([Z] - [U])[I]. \quad (4.46b)$$

Eliminating $[I]$ from (4.46a) and (4.46b) gives

$$[V^-] = ([Z] - [U])([Z] + [U])^{-1}[V^+],$$

so that

$$[S] = ([Z] - [U])([Z] + [U])^{-1}. \quad (4.47)$$

Taking the transpose of (4.47) gives

$$[S]^t = \{([Z] + [U])^{-1}\}^t ([Z] - [U])^t.$$

Now $[U]$ is diagonal, so $[U]^t = [U]$, and if the network is reciprocal, $[Z]$ is symmetric, so that $[Z]^t = [Z]$. The above equation then reduces to

$$[S]^t = ([Z] + [U])^{-1} ([Z] - [U]),$$

which is equivalent to (4.44). We have thus shown that

$$[S] = [S]^t, \quad (4.48)$$

so the scattering matrix is symmetric for reciprocal networks.

If the network is lossless, no real power can be delivered to the network. Thus, if the characteristic impedances of all the ports are identical and assumed to be unity, the average power delivered to the network is

$$\begin{aligned} P_{\text{avg}} &= \frac{1}{2} \text{Re}\{[V]^t [I]^*\} = \frac{1}{2} \text{Re}\{([V^+]^t + [V^-]^t)([V^+]^* - [V^-]^*)\} \\ &= \frac{1}{2} \text{Re}\{[V^+]^t [V^+]^* - [V^+]^t [V^-]^* + [V^-]^t [V^+]^* - [V^-]^t [V^-]^*\} \\ &= \frac{1}{2} [V^+]^t [V^+]^* - \frac{1}{2} [V^-]^t [V^-]^* = 0, \end{aligned} \quad (4.49)$$

since the terms $-[V^+]^t [V^-]^* + [V^-]^t [V^+]^*$ are of the form $A - A^*$, and so are purely imaginary. Of the remaining terms in (4.49), $(1/2)[V^+]^t [V^+]^*$ represents the total incident power, while $(1/2)[V^-]^t [V^-]^*$ represents the total reflected power. So, for a lossless junction, we have the intuitive result that the incident and reflected powers are equal:

$$[V^+]^t [V^+]^* = [V^-]^t [V^-]^*. \quad (4.50)$$

Using $[V^-] = [S][V^+]$ in (4.50) gives

$$[V^+]^t [V^+]^* = [V^+]^t [S]^t [S]^* [V^+]^*,$$

so that, for nonzero $[V^+]$,

$$[S]^t [S]^* = [U], \quad (4.51)$$

$$\text{or } [S]^* = \{[S]^t\}^{-1}.$$

A matrix that satisfies the condition of (4.51) is called a *unitary matrix*.

The matrix equation of (4.51) can be written in summation form as

$$\sum_{k=1}^N S_{ki} S_{kj}^* = \delta_{ij}, \text{ for all } i, j, \quad (4.52)$$

where $\delta_{ij} = 1$ if $i = j$, and $\delta_{ij} = 0$ if $i \neq j$, is the Kronecker delta symbol. Thus, if $i = j$, (4.52) reduces to

$$\sum_{k=1}^N S_{ki} S_{ki}^* = 1, \quad (4.53a)$$

while if $i \neq j$, (4.52) reduces to

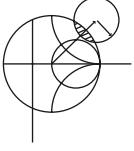
$$\sum_{k=1}^N S_{ki} S_{kj}^* = 0, \text{ for } i \neq j. \quad (4.53b)$$

In words, (4.53a) states that the dot product of any column of $[S]$ with the conjugate of that same column gives unity, while (4.53b) states that the dot product of any column with the

conjugate of a different column gives zero (the columns are orthonormal). From (4.51) we also have that

$$[S][S]^* = [U],$$

so the same statements can be made about the rows of the scattering matrix.



EXAMPLE 4.5 APPLICATION OF SCATTERING PARAMETERS

A two-port network is known to have the following scattering matrix:

$$[S] = \begin{bmatrix} 0.15 \angle 0^\circ & 0.85 \angle -45^\circ \\ 0.85 \angle 45^\circ & 0.2 \angle 0^\circ \end{bmatrix}$$

Determine if the network is reciprocal and lossless. If port 2 is terminated with a matched load, what is the return loss seen at port 1? If port 2 is terminated with a short circuit, what is the return loss seen at port 1?

Solution

Because $[S]$ is not symmetric, the network is not reciprocal. To be lossless, the scattering parameters must satisfy (4.53). Taking the first column [$i = 1$ in (4.53a)] gives

$$|S_{11}|^2 + |S_{21}|^2 = (0.15)^2 + (0.85)^2 = 0.745 \neq 1,$$

so the network is not lossless.

When port 2 is terminated with a matched load, the reflection coefficient seen at port 1 is $\Gamma = S_{11} = 0.15$. So the return loss is

$$\text{RL} = -20 \log |\Gamma| = -20 \log(0.15) = 16.5 \text{ dB}.$$

When port 2 is terminated with a short circuit, the reflection coefficient seen at port 1 can be found as follows. From the definition of the scattering matrix and the fact that $V_2^+ = -V_2^-$ (for a short circuit at port 2), we can write

$$V_1^- = S_{11} V_1^+ + S_{12} V_2^+ = S_{11} V_1^+ - S_{12} V_2^-,$$

$$V_2^- = S_{21} V_1^+ + S_{22} V_2^+ = S_{21} V_1^+ - S_{22} V_2^-.$$

The second equation gives

$$V_2^- = \frac{S_{21}}{1 + S_{22}} V_1^+.$$

Dividing the first equation by V_1^+ and using the above result gives the reflection coefficient seen at port 1 as

$$\begin{aligned} \Gamma = \frac{V_1^-}{V_1^+} &= S_{11} - S_{12} \frac{V_2^-}{V_1^+} = S_{11} - \frac{S_{12} S_{21}}{1 + S_{22}} \\ &= 0.15 - \frac{(0.85 \angle -45^\circ)(0.85 \angle 45^\circ)}{1 + 0.2} = -0.452. \end{aligned}$$

So the return loss is $\text{RL} = -20 \log |\Gamma| = -20 \log(0.452) = 6.9 \text{ dB}$. ■

An important point to understand about scattering parameters is that the reflection coefficient looking into port n is not equal to S_{nn} unless all other ports are matched (this

is illustrated in the above example). Similarly, the transmission coefficient from port m to port n is not equal to S_{nm} unless all other ports are matched. The scattering parameters of a network are properties only of the network itself (assuming the network is linear), and are defined under the condition that all ports are matched. Changing the terminations or excitations of a network does not change its scattering parameters, but may change the reflection coefficient seen at a given port, or the transmission coefficient between two ports.

A Shift in Reference Planes

Because scattering parameters relate amplitudes (magnitude and phase) of traveling waves incident on and reflected from a microwave network, phase reference planes must be specified for each port of the network. We now show how scattering parameters are transformed when the reference planes are moved from their original locations.

Consider the N -port microwave network shown in Figure 4.9, where the original terminal planes are assumed to be located at $z_n = 0$ for the n th port, where z_n is an arbitrary coordinate measured along the transmission line feeding the n th port. The scattering matrix for the network with this set of terminal planes is denoted by $[S]$. Now consider a new set of reference planes defined at $z_n = \ell_n$ for the n th port, and let the new scattering matrix be denoted as $[S']$. Then in terms of the incident and reflected port voltages we have that

$$[V^-] = [S][V^+], \quad (4.54a)$$

$$[V'^-] = [S'] [V'^+], \quad (4.54b)$$

where the unprimed quantities are referenced to the original terminal planes at $z_n = 0$, and the primed quantities are referenced to the new terminal planes at $z_n = \ell_n$.

From the theory of traveling waves on lossless transmission lines we can relate the new wave amplitudes to the original ones as

$$V_n'^+ = V_n^+ e^{j\theta_n}, \quad (4.55a)$$

$$V_n'^- = V_n^- e^{-j\theta_n}, \quad (4.55b)$$

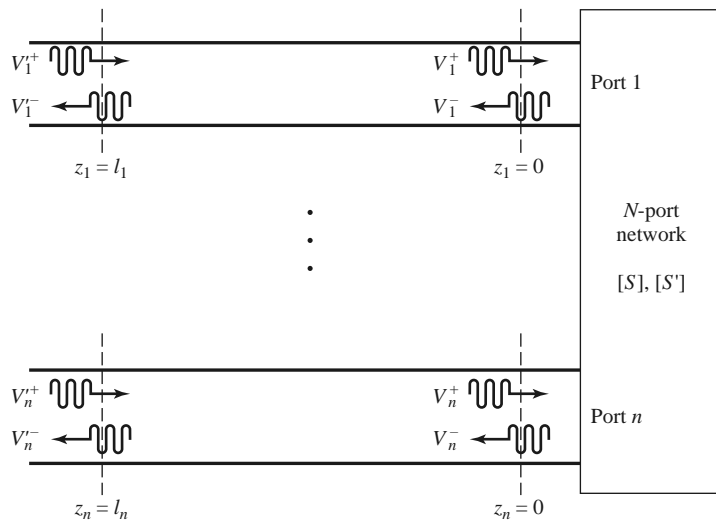


FIGURE 4.9 Shifting reference planes for an N -port network.

where $\theta_n = \beta_n \ell_n$ is the electrical length of the outward shift of the reference plane of port n . Writing (4.55) in matrix form and substituting into (4.54a) gives

$$\begin{bmatrix} e^{j\theta_1} & & 0 \\ & e^{j\theta_2} & \\ & \ddots & \\ 0 & & e^{j\theta_N} \end{bmatrix} [V'^-] = [S] \begin{bmatrix} e^{-j\theta_1} & & 0 \\ & e^{-j\theta_2} & \\ & \ddots & \\ 0 & & e^{-j\theta_N} \end{bmatrix} [V'^+].$$

Multiplying by the inverse of the first matrix on the left gives

$$[V'^-] = \begin{bmatrix} e^{-j\theta_1} & & 0 \\ & e^{-j\theta_2} & \\ & \ddots & \\ 0 & & e^{-j\theta_N} \end{bmatrix} [S] \begin{bmatrix} e^{-j\theta_1} & & 0 \\ & e^{-j\theta_2} & \\ & \ddots & \\ 0 & & e^{-j\theta_N} \end{bmatrix} [V'^+].$$

Comparing with (4.54b) shows that

$$[S'] = \begin{bmatrix} e^{-j\theta_1} & & 0 \\ & e^{-j\theta_2} & \\ & \ddots & \\ 0 & & e^{-j\theta_N} \end{bmatrix} [S] \begin{bmatrix} e^{-j\theta_1} & & 0 \\ & e^{-j\theta_2} & \\ & \ddots & \\ 0 & & e^{-j\theta_N} \end{bmatrix}, \quad (4.56)$$

which is the desired result. Note that $S'_{nn} = e^{-2j\theta_n} S_{nn}$, meaning that the phase of S_{nn} is shifted by twice the electrical length of the shift in terminal plane n because the wave travels twice over this length upon incidence and reflection. This result is consistent with (2.42), which gives the change in the reflection coefficient on a transmission line due to a shift in the reference plane.

Power Waves and Generalized Scattering Parameters

We previously expressed the total voltage and current on a transmission line in terms of the incident and reflected voltage wave amplitudes, as in (2.34) or (4.42):

$$V = V_0^+ + V_0^-, \quad (4.57a)$$

$$I = \frac{1}{Z_0} (V_0^+ - V_0^-), \quad (4.57b)$$

with Z_0 being the characteristic impedance of the line. Inverting (4.57) gives the incident and reflected voltage wave amplitudes in terms of the total voltage and current:

$$V_0^+ = \frac{V + Z_0 I}{2}, \quad (4.58a)$$

$$V_0^- = \frac{V - Z_0 I}{2}. \quad (4.58b)$$

The average power delivered to a load can be expressed as

$$\begin{aligned} P_L &= \frac{1}{2} \operatorname{Re} \{ V I^* \} = \frac{1}{2Z_0} \operatorname{Re} \left\{ |V_0^+|^2 - V_0^+ V_0^{-*} + V_0^{+*} V_0^- - |V_0^-|^2 \right\} \\ &= \frac{1}{2Z_0} (|V_0^+|^2 - |V_0^-|^2), \end{aligned} \quad (4.59)$$

where the last step follows because the quantity $V_0^{+*} V_0^- - V_0^+ V_0^{-*}$ is pure imaginary. This is a physically satisfying result since it expresses the net power delivered to the load as the difference between the incident and reflected powers. Unfortunately, this result is only

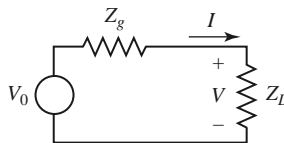


FIGURE 4.10 A generator with impedance Z_g connected to a load impedance Z_L .

valid when the characteristic impedance is real; it does not apply when Z_0 is complex, as in the case of a lossy line. In addition, these results are not useful when no transmission line is present between the generator and load, as in the circuit shown in Figure 4.10.

In the circuit of Figure 4.10 there is no defined characteristic impedance, nor is there a voltage reflection coefficient, or incident and reflected voltage or current waves. It is possible, however, to define a new set of waves, called *power waves*, which have useful properties when dealing with power transfer between a generator and a load, and can be applied to circuits like that of Figure 4.10, as well as to problems with lossless or lossy transmission lines. We will also see how power waves lead to a generalization of scattering parameters.

The incident and reflected power wave amplitudes a and b are defined as the following linear transformations of the total voltage and current:

$$a = \frac{V + Z_R I}{2\sqrt{R_R}}, \quad (4.60a)$$

$$b = \frac{V - Z_R^* I}{2\sqrt{R_R}}, \quad (4.60b)$$

where $Z_R = R_R + jX_R$ is known as the *reference impedance*, and may be complex. Note that the power wave amplitudes of (4.60) are similar in form to the voltage waves of (4.58), but do not have units of power, voltage, or current.

Inverting (4.60) gives the total voltage and current in terms of the power wave amplitudes:

$$V = \frac{Z_R^* a + Z_R b}{\sqrt{R_R}}, \quad (4.61a)$$

$$I = \frac{a - b}{\sqrt{R_R}}. \quad (4.61b)$$

Then the power delivered to the load can be expressed as

$$\begin{aligned} P_L &= \frac{1}{2} \operatorname{Re} \{ V I^* \} = \frac{1}{2R_R} \operatorname{Re} \left\{ Z_R^* |a|^2 - Z_R^* a b^* + Z_R a^* b - Z_R |b|^2 \right\} \\ &= \frac{1}{2} |a|^2 - \frac{1}{2} |b|^2, \end{aligned} \quad (4.62)$$

since the quantity $Z_R a^* b - Z_R^* a b^*$ is pure imaginary. Once again we have the satisfying result that the load power is the difference between the powers of the incident and reflected power waves. It is important to note that this result is valid for any reference impedance Z_R .

The reflection coefficient, Γ_p , for the reflected power wave can be found by using (4.60) and the fact that $V = Z_L I$ at the load:

$$\Gamma_p = \frac{b}{a} = \frac{V - Z_R^* I}{V + Z_R I} = \frac{Z_L - Z_R^*}{Z_L + Z_R}. \quad (4.63)$$

Observe that this reflection coefficient reduces to our usual voltage reflection coefficient of (2.35) when $Z_R = Z_0$ is a real characteristic impedance. Equation (4.63) suggests that

choosing the reference impedance as the conjugate of the load impedance [5],

$$Z_R = Z_L^*, \quad (4.64)$$

will have the useful effect of making the reflected power wave amplitude go to zero.¹

From basic circuit theory, the voltage, current, and load power for the circuit of Figure 4.10 are

$$V = V_0 \frac{Z_L}{Z_L + Z_g}, \quad I = \frac{V_0}{Z_L + Z_g}, \quad P_L = \frac{V_0^2}{2} \frac{R_L}{|Z_L + Z_g|^2}, \quad (4.65a, b, c)$$

where $Z_L = R_L + jX_L$. Then the power wave amplitudes can be found from (4.60), with $Z_R = Z_L^*$, as

$$a = \frac{V + Z_R I}{2\sqrt{R_R}} = V_0 \frac{\frac{Z_L}{Z_L + Z_g} + \frac{Z_L^*}{Z_L + Z_g}}{2\sqrt{R_R}} = V_0 \frac{\sqrt{R_L}}{Z_L + Z_g}, \quad (4.66a)$$

$$b = \frac{V - Z_R^* I}{2\sqrt{R_R}} = V_0 \frac{\frac{Z_L}{Z_L + Z_g} - \frac{Z_L}{Z_L + Z_g}}{2\sqrt{R_R}} = 0. \quad (4.66b)$$

From (4.62) the power delivered to the load is

$$P_L = \frac{1}{2} |a|^2 = \frac{V_0^2}{2} \frac{R_L}{|Z_L + Z_g|^2},$$

in agreement with (4.65c).

When the load is conjugately matched to the generator, so that $Z_g = Z_L^*$, we have $P_L = V_0^2/8R_L$. Note that selecting the reference impedance as $Z_R = Z_L^*$ results in the condition that $b = 0$ (and $\Gamma_p = 0$), but this does not necessarily mean that the load is conjugately matched to the generator, nor that maximum power is delivered to the load. The incident power wave amplitude of (4.66a) depends on Z_L and Z_g , and is maximum only when $Z_g = Z_L^*$.

To define the scattering matrix for power waves for an N -port network, we assume the reference impedance for port i is Z_{Ri} . Then, analogous to (4.60), we define the power wave amplitude vectors in terms of the total voltage and current vectors:

$$[a] = [F] ([V] + [Z_R] [I]), \quad (4.67a)$$

$$[b] = [F] ([V] - [Z_R]^* [I]), \quad (4.67b)$$

where $[F]$ is a diagonal matrix with elements $1/2\sqrt{\text{Re}\{Z_{Ri}\}}$ and $[Z_R]$ is a diagonal matrix with elements Z_{Ri} . By the impedance matrix relation that $[V] = [Z][I]$, (4.67) can be written as

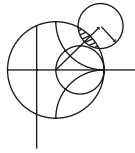
$$[b] = [F] ([Z] - [Z_R]^*) ([Z] + [Z_R])^{-1} [F]^{-1} [a].$$

Because the scattering matrix for power waves, $[S_p]$, should relate $[b]$ to $[a]$, we have

$$[S_p] = [F] ([Z] - [Z_R]^*) ([Z] + [Z_R])^{-1} [F]^{-1}. \quad (4.68)$$

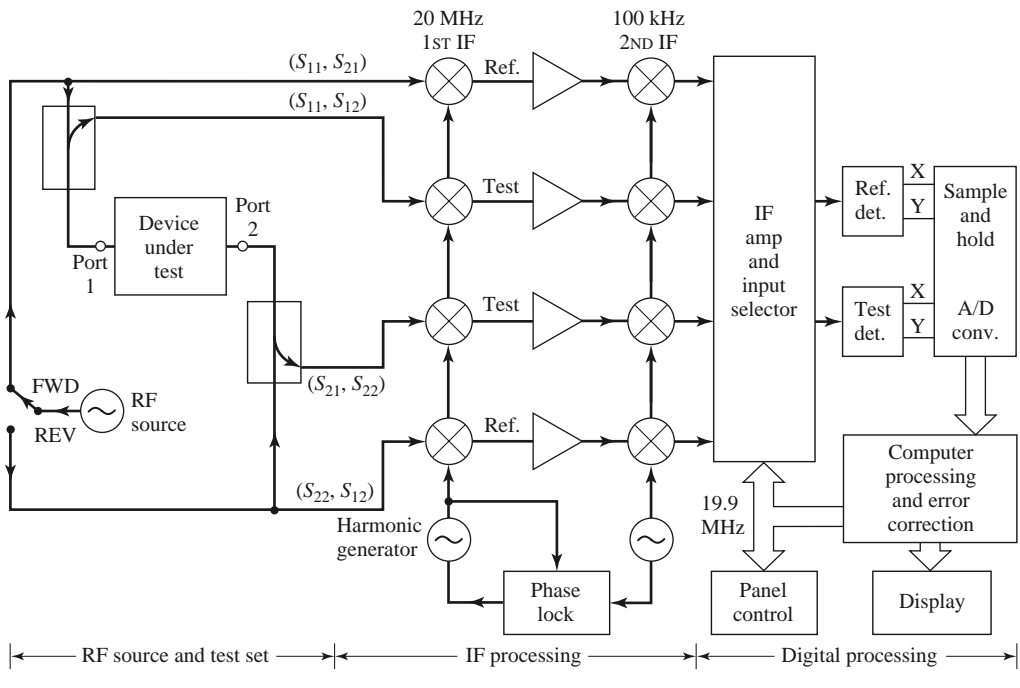
¹ Some authors choose the reference impedance equal to the generator impedance. This has the same effect as (4.64) when the generator and load are conjugately matched, but the choice of (4.64) leads to a zero reflected wave even when the conjugate matching condition is not satisfied, and so can be more useful in general.

The ordinary scattering matrix for a network can first be converted to an impedance matrix, using a relation similar to (4.45), then converted to the generalized power wave scattering matrix using (4.68). The generalized scattering matrix has the useful property that the diagonal elements can be made to be zero by proper selection of the reference impedances.



POINT OF INTEREST: The Vector Network Analyzer

The scattering parameters of passive and active networks can be measured with a *vector network analyzer*, which is a two-channel (or four-channel) microwave receiver designed to process the magnitude and phase of the transmitted and reflected waves from the network. A simplified block diagram of a network analyzer is shown in the accompanying figure. In operation, the RF source is usually set to sweep over a specified bandwidth. A four-port reflectometer samples the incident, reflected, and transmitted RF waves; a switch allows the network to be driven from either port 1 or port 2. Four dual-conversion channels convert these signals to 100-kHz IF frequencies, which are then detected and converted to digital form. An internal computer is used to calculate and display the magnitude and phase of the scattering parameters or other quantities that can be derived from these data, such as SWR, return loss, group delay, impedance, etc. An important feature of the network analyzer is the substantial improvement in accuracy made possible with error-correcting software. Errors caused by directional coupler mismatch, imperfect directivity, loss, and variations in the frequency response of the analyzer system are accounted for by using a 12-term error model and a calibration procedure. Another useful feature is the ability to determine the time-domain response of the network by calculating the inverse Fourier transform of the frequency-domain data.



4.4 THE TRANSMISSION (ABCD) MATRIX

The Z , Y , and S parameter representations can be used to characterize a microwave network with an arbitrary number of ports, but in practice many microwave networks consist of a cascade connection of two or more two-port networks. In this case it is convenient

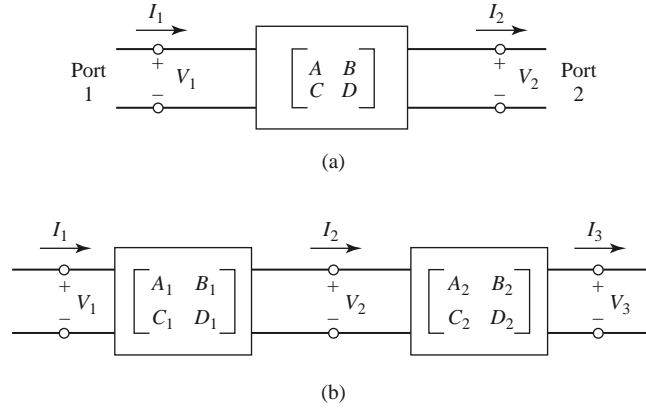


FIGURE 4.11 (a) A two-port network; (b) a cascade connection of two-port networks.

to define a 2×2 *transmission*, or *ABCD*, *matrix*, for each two-port network. We will see that the *ABCD* matrix of the cascade connection of two or more two-port networks can be easily found by multiplying the *ABCD* matrices of the individual two-ports.

The *ABCD* matrix is defined for a two-port network in terms of the total voltages and currents as shown in Figure 4.11a and the following:

$$V_1 = AV_2 + BI_2,$$

$$I_1 = CV_2 + DI_2,$$

or in matrix form as

$$\begin{bmatrix} V_1 \\ I_1 \end{bmatrix} = \begin{bmatrix} A & B \\ C & D \end{bmatrix} \begin{bmatrix} V_2 \\ I_2 \end{bmatrix}. \quad (4.69)$$

It is important to note from Figure 4.11a that a change in the sign convention of I_2 has been made from our previous definitions, which had I_2 as the current flowing *into* port 2. The convention that I_2 flows *out* of port 2 will be used when dealing with *ABCD* matrices so that in a cascade network I_2 will be the same current that flows into the adjacent network, as shown in Figure 4.11b. Then the left-hand side of (4.69) represents the voltage and current at port 1 of the network, while the column on the right-hand side of (4.69) represents the voltage and current at port 2.

In the cascade connection of two two-port networks shown in Figure 4.11b we have that

$$\begin{bmatrix} V_1 \\ I_1 \end{bmatrix} = \begin{bmatrix} A_1 & B_1 \\ C_1 & D_1 \end{bmatrix} \begin{bmatrix} V_2 \\ I_2 \end{bmatrix}, \quad (4.70a)$$

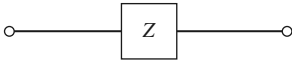
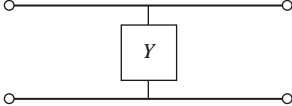
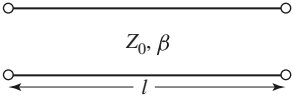
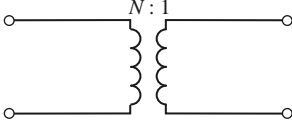
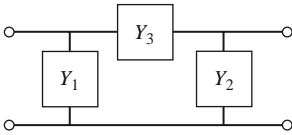
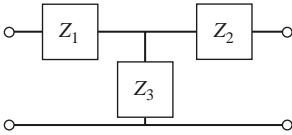
$$\begin{bmatrix} V_2 \\ I_2 \end{bmatrix} = \begin{bmatrix} A_2 & B_2 \\ C_2 & D_2 \end{bmatrix} \begin{bmatrix} V_3 \\ I_3 \end{bmatrix}.$$

Substituting (4.70b) into (4.70a) gives

$$\begin{bmatrix} V_1 \\ I_1 \end{bmatrix} = \begin{bmatrix} A_1 & B_1 \\ C_1 & D_1 \end{bmatrix} \begin{bmatrix} A_2 & B_2 \\ C_2 & D_2 \end{bmatrix} \begin{bmatrix} V_3 \\ I_3 \end{bmatrix}, \quad (4.71)$$

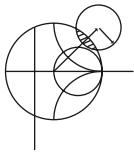
which shows that the *ABCD* matrix of the cascade connection of the two networks is equal to the product of the *ABCD* matrices representing the individual two-ports. Note that the

TABLE 4.1 *ABCD* Parameters of Some Useful Two-Port Circuits

| Circuit | <i>ABCD</i> Parameters | |
|---|--|--|
|  | $A = 1$ $C = 0$ | $B = Z$ $D = 1$ |
|  | $A = 1$ $C = Y$ | $B = 0$ $D = 1$ |
|  | $A = \cos \beta \ell$ $C = jY_0 \sin \beta \ell$ | $B = jZ_0 \sin \beta \ell$ $D = \cos \beta \ell$ |
|  | $A = N$ $C = 0$ | $B = 0$ $D = \frac{1}{N}$ |
|  | $A = 1 + \frac{Y_2}{Y_3}$ $C = Y_1 + Y_2 + \frac{Y_1 Y_2}{Y_3}$ | $B = \frac{1}{Y_3}$ $D = 1 + \frac{Y_1}{Y_3}$ |
|  | $A = 1 + \frac{Z_1}{Z_3}$ $C = \frac{1}{Z_3}$ | $B = Z_1 + Z_2 + \frac{Z_1 Z_2}{Z_3}$ $D = 1 + \frac{Z_2}{Z_3}$ |

order of multiplication of the matrix must be the same as the order in which the networks are arranged since matrix multiplication is not, in general, commutative.

The usefulness of the *ABCD* matrix representation lies in the fact that a library of *ABCD* matrices for elementary two-port networks can be built up, and applied in building-block fashion to more complicated microwave networks that consist of cascades of these simpler two-ports. Table 4.1 lists a number of useful two-port networks and their *ABCD* matrices.



EXAMPLE 4.6 EVALUATION OF *ABCD* PARAMETERS

Find the *ABCD* parameters of a two-port network consisting of a series impedance *Z* between ports 1 and 2 (the first entry in Table 4.1).

Solution

From the defining relations of (4.69), we have that

$$A = \left. \frac{V_1}{V_2} \right|_{I_2=0},$$

which indicates that A is found by applying a voltage V_1 at port 1, and measuring the open-circuit voltage V_2 at port 2. Thus, $A = 1$. Similarly,

$$B = \left. \frac{V_1}{I_2} \right|_{V_2=0} = \frac{V_1}{V_1/Z} = Z,$$

$$C = \left. \frac{I_1}{V_2} \right|_{I_2=0} = 0,$$

$$D = \left. \frac{I_1}{I_2} \right|_{V_2=0} = \frac{I_1}{I_1} = 1. \quad \blacksquare$$

Relation to Impedance Matrix

The impedance parameters of a network can be easily converted to *ABCD* parameters. Thus, from the definition of the *ABCD* parameters in (4.69), and from the defining relations for the Z parameters of (4.25) for a two-port network with I_2 to be consistent with the sign convention used with *ABCD* parameters,

$$V_1 = I_1 Z_{11} - I_2 Z_{12}, \quad (4.72a)$$

$$V_2 = I_1 Z_{21} - I_2 Z_{22}, \quad (4.72b)$$

we have that

$$A = \left. \frac{V_1}{V_2} \right|_{I_2=0} = \frac{I_1 Z_{11}}{I_1 Z_{21}} = Z_{11}/Z_{21}, \quad (4.73a)$$

$$\begin{aligned} B &= \left. \frac{V_1}{I_2} \right|_{V_2=0} = \left. \frac{I_1 Z_{11} - I_2 Z_{12}}{I_2} \right|_{V_2=0} = Z_{11} \left. \frac{I_1}{I_2} \right|_{V_2=0} - Z_{12} \\ &= Z_{11} \frac{I_1 Z_{22}}{I_1 Z_{21}} - Z_{12} = \frac{Z_{11} Z_{22} - Z_{12} Z_{21}}{Z_{21}}, \end{aligned} \quad (4.73b)$$

$$C = \left. \frac{I_1}{V_2} \right|_{I_2=0} = \frac{I_1}{I_1 Z_{21}} = 1/Z_{21}, \quad (4.73c)$$

$$D = \left. \frac{I_1}{I_2} \right|_{V_2=0} = \frac{I_2 Z_{22}/Z_{21}}{I_2} = Z_{22}/Z_{21}. \quad (4.73d)$$

If the network is reciprocal, then $Z_{12} = Z_{21}$ and (4.73) can be used to show that $AD - BC = 1$.

Equivalent Circuits for Two-Port Networks

The special case of a two-port microwave network occurs so frequently in practice that it deserves further attention. Here we will discuss the use of equivalent circuits to represent an arbitrary two-port network. Useful conversions between two-port network parameters are given in Table 4.2.

Figure 4.12a shows a transition between a coaxial line and a microstrip line, and is an example of a two-port network. Terminal planes can be defined at arbitrary points on the two transmission lines; a convenient choice might be as shown in the figure. However, because of the physical discontinuity in the transition from a coaxial line to a microstrip line, electric and/or magnetic energy can be stored in the vicinity of the junction, leading to reactive effects. Characterization of such effects can be obtained by measurement or by numerical analysis (such analysis may be quite complicated), and represented by the

TABLE 4.2 Conversions Between Two-Port Network Parameters

| | S | Z | Y | ABCD |
|--|---|--|--|--|
| S_{11} | S_{11} | $\frac{(Z_{11} - Z_0)(Z_{22} + Z_0) - Z_{12}Z_{21}}{\Delta Z}$ | $\frac{(Y_0 - Y_{11})(Y_0 + Y_{22}) + Y_{12}Y_{21}}{\Delta Y}$ | $\frac{A + B/Z_0 - CZ_0 - D}{A + B/Z_0 + CZ_0 + D}$ |
| S_{12} | S_{12} | $\frac{2Z_{12}Z_0}{\Delta Z}$ | $\frac{-2Y_{12}Y_0}{\Delta Y}$ | $\frac{2(AD - BC)}{A + B/Z_0 + CZ_0 + D}$ |
| S_{21} | S_{21} | $\frac{2Z_{21}Z_0}{\Delta Z}$ | $\frac{-2Y_{21}Y_0}{\Delta Y}$ | $\frac{2}{A + B/Z_0 + CZ_0 + D}$ |
| S_{22} | S_{22} | $\frac{(Z_{11} + Z_0)(Z_{22} - Z_0) - Z_{12}Z_{21}}{\Delta Z}$ | $\frac{(Y_0 + Y_{11})(Y_0 - Y_{22}) + Y_{12}Y_{21}}{\Delta Y}$ | $\frac{-A + B/Z_0 - CZ_0 + D}{A + B/Z_0 + CZ_0 + D}$ |
| Z_{11} | $Z_0 \frac{(1 + S_{11})(1 - S_{22}) + S_{12}S_{21}}{(1 - S_{11})(1 - S_{22}) - S_{12}S_{21}}$ | Z_{11} | $\frac{Y_{22}}{ Y }$ | $\frac{A}{C}$ |
| Z_{12} | $Z_0 \frac{2S_{12}}{(1 - S_{11})(1 - S_{22}) - S_{12}S_{21}}$ | Z_{12} | $\frac{-Y_{12}}{ Y }$ | $\frac{AD - BC}{C}$ |
| Z_{21} | $Z_0 \frac{2S_{21}}{(1 - S_{11})(1 - S_{22}) - S_{12}S_{21}}$ | Z_{21} | $\frac{-Y_{21}}{ Y }$ | $\frac{1}{C}$ |
| Z_{22} | $Z_0 \frac{(1 - S_{11})(1 + S_{22}) + S_{12}S_{21}}{(1 - S_{11})(1 - S_{22}) + S_{12}S_{21}}$ | Z_{22} | $\frac{Y_{11}}{ Y }$ | $\frac{D}{C}$ |
| Y_{11} | $Y_0 \frac{(1 - S_{11})(1 + S_{22}) + S_{12}S_{21}}{(1 + S_{11})(1 + S_{22}) - S_{12}S_{21}}$ | $\frac{Z_{22}}{ Z }$ | Y_{11} | $\frac{D}{B}$ |
| Y_{12} | $Y_0 \frac{-2S_{12}}{(1 + S_{11})(1 + S_{22}) - S_{12}S_{21}}$ | $\frac{-Z_{12}}{ Z }$ | Y_{12} | $\frac{BC - AD}{B}$ |
| Y_{21} | $Y_0 \frac{-2S_{21}}{(1 + S_{11})(1 + S_{22}) - S_{12}S_{21}}$ | $\frac{-Z_{21}}{ Z }$ | Y_{21} | $\frac{-1}{B}$ |
| Y_{22} | $Y_0 \frac{(1 + S_{11})(1 - S_{22}) + S_{12}S_{21}}{(1 + S_{11})(1 + S_{22}) - S_{12}S_{21}}$ | $\frac{Z_{11}}{ Z }$ | Y_{22} | $\frac{A}{B}$ |
| A | $\frac{(1 + S_{11})(1 - S_{22}) + S_{12}S_{21}}{2S_{21}}$ | $\frac{Z_{11}}{Z_{21}}$ | $\frac{-Y_{22}}{Y_{21}}$ | A |
| B | $Z_0 \frac{(1 + S_{11})(1 + S_{22}) - S_{12}S_{21}}{2S_{21}}$ | $\frac{ Z }{Z_{21}}$ | $\frac{-1}{Y_{21}}$ | B |
| C | $\frac{1}{Z_0} \frac{(1 - S_{11})(1 - S_{22}) - S_{12}S_{21}}{2S_{21}}$ | $\frac{1}{Z_{21}}$ | $\frac{- Y }{Y_{21}}$ | C |
| D | $\frac{(1 - S_{11})(1 + S_{22}) + S_{12}S_{21}}{2S_{21}}$ | $\frac{Z_{22}}{Z_{21}}$ | $\frac{-Y_{11}}{Y_{21}}$ | D |
| $ Z = Z_{11}Z_{22} - Z_{12}Z_{21}; \quad Y = Y_{11}Y_{22} - Y_{12}Y_{21}; \quad \Delta Y = (Y_{11} + Y_0)(Y_{22} + Y_0) - Y_{12}Y_{21}; \quad \Delta Z = (Z_{11} + Z_0)(Z_{22} + Z_0) - Z_{12}Z_{21}; \quad Y_0 = 1/Z_0.$ | | | | |

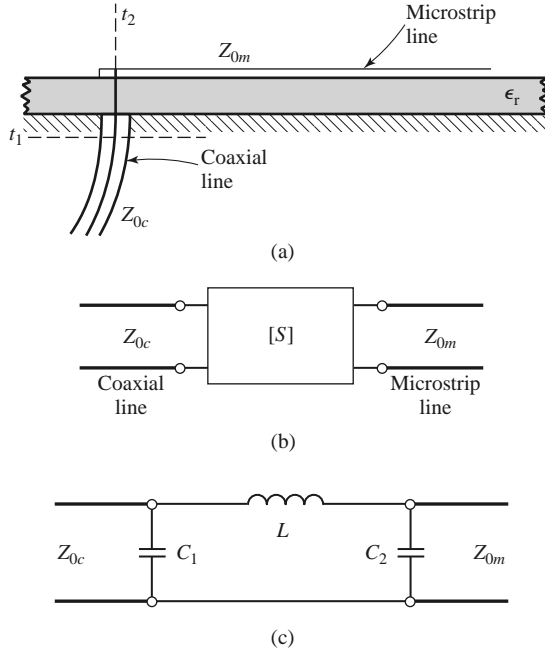


FIGURE 4.12 A coax-to-microstrip transition and equivalent circuit representations. (a) Geometry of the transition. (b) Representation of the transition by a “black box.” (c) A possible equivalent circuit for the transition [6].

two-port “black box” shown in Figure 4.12b. The properties of the transition can then be expressed in terms of the network parameters (Z , Y , S , or $ABCD$) of the two-port network. This type of treatment can be applied to a variety of two-port junctions, such as transitions from one type of transmission line to another, transmission line discontinuities such as step changes in width or bends, etc. When modeling a microwave junction in this way, it is often useful to replace the two-port “black box” with an equivalent circuit containing a few idealized components, as shown in Figure 4.12c. This is particularly useful if the component values can be related to some physical features of the actual junction. There is an unlimited number of ways in which such equivalent circuits can be defined; we will discuss some of the most common and useful types below.

As we have seen, an arbitrary two-port network can be described in terms of impedance parameters as

$$\begin{aligned} V_1 &= Z_{11}I_1 + Z_{12}I_2, \\ V_2 &= Z_{21}I_1 + Z_{22}I_2, \end{aligned} \quad (4.74a)$$

or in terms of admittance parameters as

$$\begin{aligned} I_1 &= Y_{11}V_1 + Y_{12}V_2, \\ I_2 &= Y_{21}V_1 + Y_{22}V_2. \end{aligned} \quad (4.74b)$$

If the network is reciprocal, then $Z_{12} = Z_{21}$ and $Y_{12} = Y_{21}$. These representations lead naturally to the T and π equivalent circuits shown in Figures 4.13a and 4.13b. The relations in Table 4.2 can be used to relate the component values to other network parameters.

Other equivalent circuits can also be used to represent a two-port network. If the network is reciprocal, there are six degrees of freedom (the real and imaginary parts of three matrix elements), so the equivalent circuit should have six independent parameters.

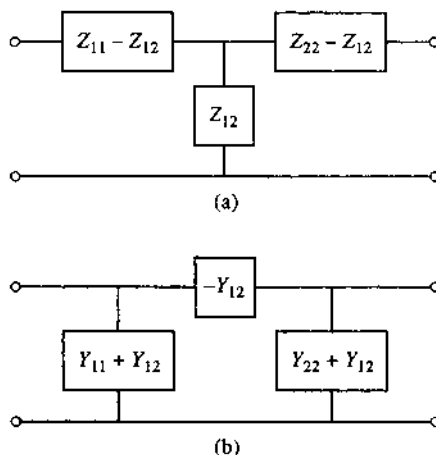


FIGURE 4.13 Equivalent circuits for a reciprocal two-port network. (a) T equivalent. (b) π equivalent.

A nonreciprocal network cannot be represented by a passive equivalent circuit using reciprocal elements.

If the network is lossless, which is a good approximation for many practical two-port junctions, some simplifications can be made in the equivalent circuit. As was shown in Section 4.2, the impedance or admittance matrix elements are purely imaginary for a lossless network. This reduces the degrees of freedom for such a network to three, and implies that the T and π equivalent circuits of Figure 4.13 can be constructed from purely reactive elements.

4.5

SIGNAL FLOW GRAPHS

We have seen how transmitted and reflected waves can be represented by scattering parameters, and how the interconnection of sources, networks, and loads can be treated with various matrix representations. In this section we discuss the *signal flow graph*, which is an additional technique that is very useful for the analysis of microwave networks in terms of transmitted and reflected waves. We first discuss the features and the construction of the flow graph itself, and then present a technique for the reduction, or solution, of the flow graph.

The primary components of a signal flow graph are nodes and branches:

- **Nodes:** Each port i of a microwave network has two nodes, a_i and b_i . Node a_i is identified with a wave entering port i , while node b_i is identified with a wave reflected from port i . The voltage at a node is equal to the sum of all signals entering that node.
- **Branches:** A branch is a directed path between two nodes representing signal flow from one node to another. Every branch has an associated scattering parameter or reflection coefficient.

At this point it is useful to consider the flow graph of an arbitrary two-port network, as shown in Figure 4.14. Figure 4.14a shows a two-port network with incident and reflected waves at each port, and Figure 4.14b shows the corresponding signal flow graph representation. The flow graph gives an intuitive graphical illustration of the network behavior.

For example, a wave of amplitude a_1 incident at port 1 is split, with part going through S_{11} and out port 1 as a reflected wave, and part transmitted through S_{21} to node b_2 .

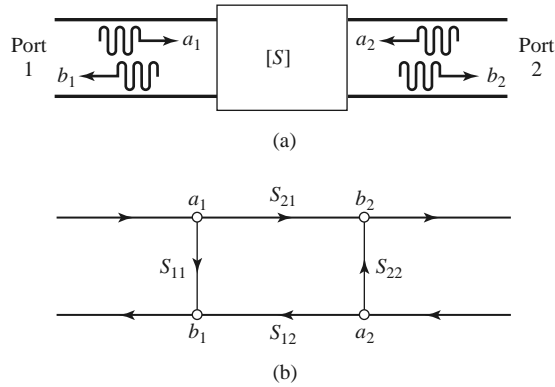


FIGURE 4.14 The signal flow graph representation of a two-port network. (a) Definition of incident and reflected waves. (b) Signal flow graph.

At node b_2 , the wave goes out port 2; if a load with nonzero reflection coefficient is connected at port 2, this wave will be at least partly reflected and reenter the two-port network at node a_2 . Part of this wave can be reflected back out port 2 via S_{22} , and part can be transmitted out port 1 through S_{12} .

Two other special networks—a one-port network and a voltage source—are shown in Figure 4.15, along with their signal flow graph representations. Once a microwave network has been represented in signal flow graph form, it is a relatively easy matter to solve for the ratio of any combination of wave amplitudes. We will discuss how this can be done using four basic decomposition rules, but the same results can also be obtained using Mason's rule from control system theory.

Decomposition of Signal Flow Graphs

A signal flow graph can be reduced to a single branch between two nodes using the following four basic decomposition rules to obtain any desired wave amplitude ratio.

- **Rule 1 (Series Rule).** Two branches, whose common node has only one incoming and one outgoing wave (branches in series), may be combined to form a single branch whose coefficient is the product of the coefficients of the original branches.

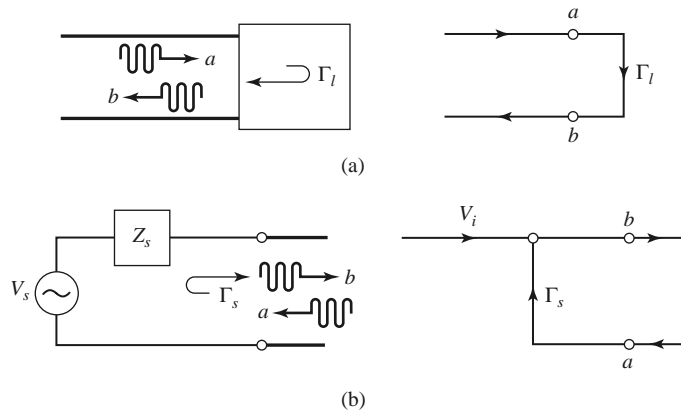


FIGURE 4.15 The signal flow graph representations of a one-port network and a source. (a) A one-port network and its flow graph. (b) A source and its flow graph.

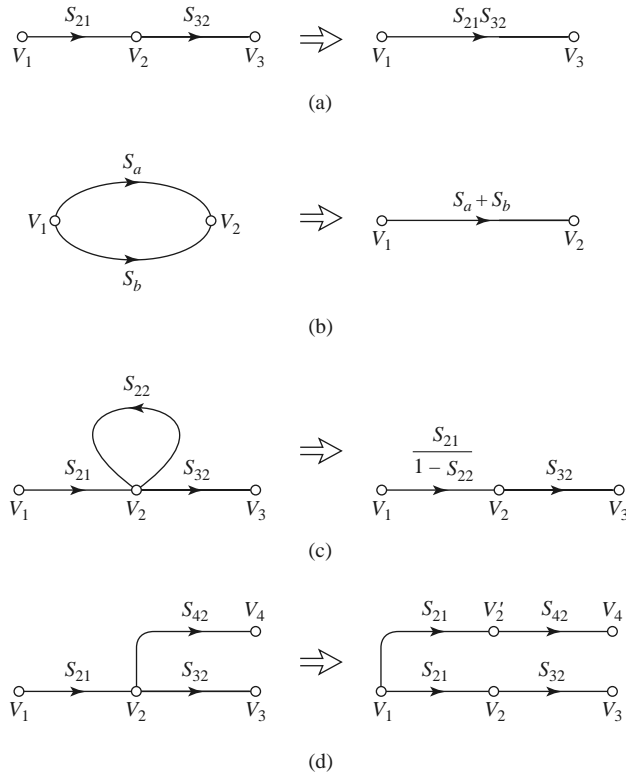


FIGURE 4.16 Decomposition rules. (a) Series rule. (b) Parallel rule. (c) Self-loop rule. (d) Splitting rule.

Figure 4.16a shows the flow graphs for this rule. Its derivation follows from the basic relation

$$V_3 = S_{32} V_2 = S_{32} S_{21} V_1. \quad (4.75)$$

- **Rule 2 (Parallel Rule).** Two branches from one common node to another common node (branches in parallel) may be combined into a single branch whose coefficient is the sum of the coefficients of the original branches. Figure 4.16b shows the flow graphs for this rule. The derivation follows from the obvious relation

$$V_2 = S_a V_1 + S_b V_1 = (S_a + S_b) V_1. \quad (4.76)$$

- **Rule 3 (Self-Loop Rule).** When a node has a self-loop (a branch that begins and ends on the same node) of coefficient S , the self-loop can be eliminated by multiplying coefficients of the branches feeding that node by $1/(1 - S)$. Figure 4.16c shows the flow graphs for this rule, which can be derived as follows. From the original network we have

$$V_2 = S_{21} V_1 + S_{22} V_2, \quad (4.77a)$$

$$V_3 = S_{32} V_2. \quad (4.77b)$$

Eliminating V_2 gives

$$V_3 = \frac{S_{32} S_{21}}{1 - S_{22}} V_1, \quad (4.78)$$

which is seen to be the transfer function for the reduced graph of Figure 4.16c.

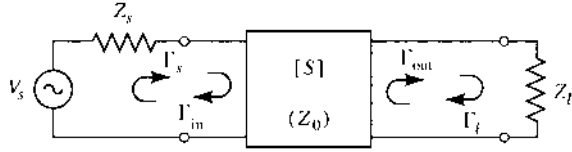


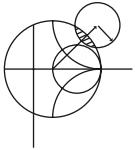
FIGURE 4.17 A terminated two-port network.

- **Rule 4 (Splitting Rule).** A node may be split into two separate nodes as long as the resulting flow graph contains, once and only once, each combination of separate (not self-loops) input and output branches that connect to the original node. This rule is illustrated in Figure 4.16d and follows from the observation that

$$V_4 = S_{42}V_2 = S_{21}S_{42}V_1 \quad (4.79)$$

in both the original flow graph and the flow graph with the split node.

We now illustrate the use of each of these rules with an example.



EXAMPLE 4.7 APPLICATION OF SIGNAL FLOW GRAPH

Use signal flow graphs to derive expressions for Γ_{in} and Γ_{out} for the microwave network shown in Figure 4.17.

Solution

The signal flow graph for the circuit of Figure 4.17 is shown in Figure 4.18. In terms of node voltages, Γ_{in} is given by the ratio b_1/a_1 . The first two steps of the required decomposition of the flow graph are shown in Figures 4.19a and 4.19b, from which the desired result follows by inspection:

$$\Gamma_{in} = \frac{b_1}{a_1} = S_{11} + \frac{S_{12}S_{21}\Gamma_L}{1 - S_{22}\Gamma_L}.$$

Next, Γ_{out} is given by the ratio b_2/a_2 . The first two steps for this decomposition are shown in Figures 4.19c and 4.19d. The desired result is

$$\Gamma_{out} = \frac{b_2}{a_2} = S_{22} + \frac{S_{12}S_{21}\Gamma_s}{1 - S_{11}\Gamma_s} \quad \blacksquare$$

Application to Thru-Reflect-Lin Network Analyzer Calibration

As a further application of signal flow graphs we consider the calibration of a network analyzer using the *Thru-Reflect-Line* (TRL) technique [7]. The general problem is shown in Figure 4.20, where it is intended to measure the scattering parameters of a two-port device

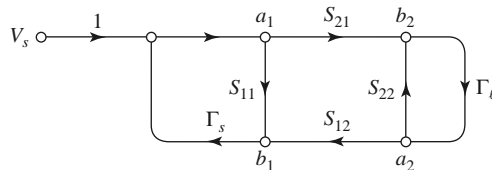


FIGURE 4.18 Signal flow graph for the two-port network with general source and load impedances of Figure 4.17.

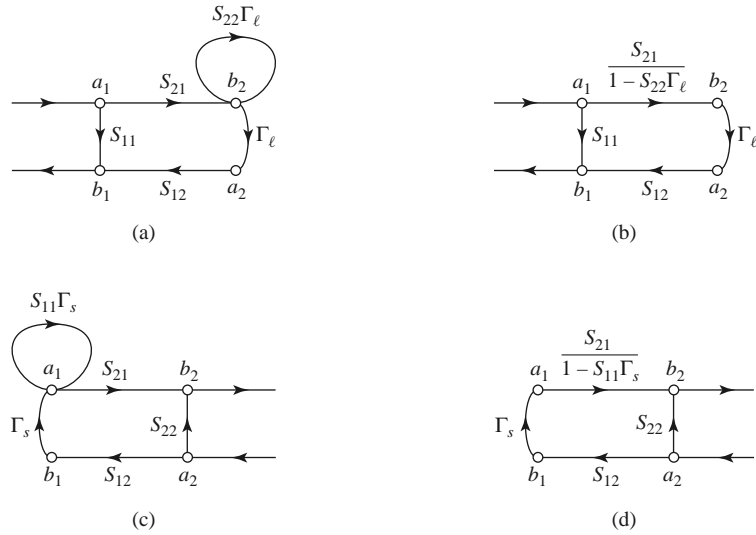


FIGURE 4.19 Decompositions of the flow graph of Figure 4.18 to find $\Gamma_{\text{in}} = b_1/a_1$ and $\Gamma_{\text{out}} = b_2/a_2$. (a) Using Rule 4 on node a_2 . (b) Using Rule 3 for the self-loop at node b_2 . (c) Using Rule 4 on node b_1 . (d) Using Rule 3 for the self-loop at node a_1 .

at the indicated reference planes. As discussed in the previous Point of Interest, a network analyzer measures scattering parameters as ratios of complex voltage amplitudes. The primary reference plane for such measurements is generally at some point within the analyzer itself, so the measurement will include losses and phase delays caused by the effects of the connectors, cables, and transitions that must be used to connect the device under test (DUT) to the analyzer. In the block diagram of Figure 4.20 these effects are lumped together in a two-port *error box* placed at each port between the actual measurement reference plane and the desired reference plane for the two-port DUT. A calibration procedure is used to characterize the error boxes before measurement of the DUT; then the actual error-corrected scattering parameters of the DUT can be calculated from the measured data. Measurement of a one-port network can be considered as a reduced version of the two-port case.

The simplest way to calibrate a network analyzer is to use three or more known loads, such as shorts, opens, and matched loads. The problem with this approach is that such standards are always imperfect to some degree, and therefore introduce errors into the measurement. These errors become increasingly significant at higher frequencies and as the quality of the measurement system improves. The TRL calibration scheme does not

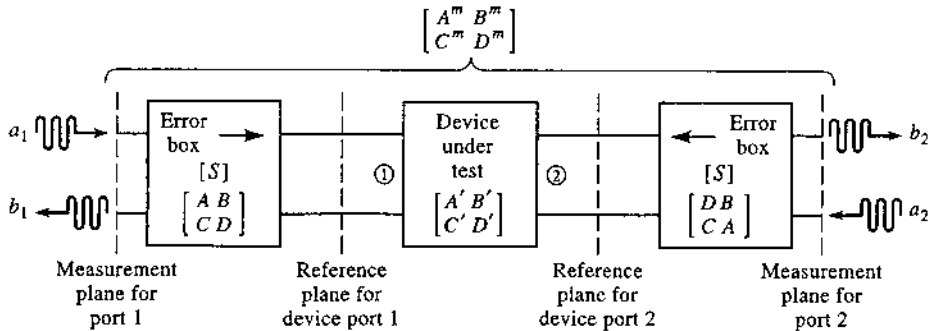


FIGURE 4.20 Block diagram of a network analyzer measurement of a two-port device.

rely on known standard loads, but uses three simple connections to allow the error boxes to be characterized completely. These three connections are shown in Figure 4.21. The *Thru* connection is made by directly connecting port 1 to port 2 at the desired reference planes. The *Reflect* connection uses a load having a large reflection coefficient, Γ_L , such as a nominal open or short. It is not necessary to know the exact value of Γ_L , as this will be determined by the TRL calibration procedure. The *Line* connection involves connecting ports 1 and 3 together through a length of matched transmission line. It is not necessary to know the length of the line, and it is not required that the line be lossless; these parameters will be determined by the TRL procedure.

We can use signal flow graphs to derive the set of equations necessary to find the scattering parameters for the error boxes in the TRL calibration procedure. With reference to Figure 4.20, we will apply the *Thru*, *Reflect*, and *Line* connections at the reference plane for the DUT, and measure the scattering parameters for these three cases at the measurement planes. For simplicity, we assume the same characteristic impedance for ports 1 and 2, and that the error boxes are reciprocal and identical for both ports. The error boxes are characterized by a scattering matrix $[S]$ and, alternatively, by an $ABCD$ matrix. Thus $S_{21} = S_{12}$ for both error boxes. Also note that ports 1 and 2 of the error boxes are in opposite positions since they are symmetrically connected, as shown in the figure. To avoid confusion in notation we will denote the measured scattering parameters for the *Thru*, *Reflect*, and *Line* connections as the $[T]$, $[R]$, and $[L]$ matrices, respectively.

Figure 4.21a shows the arrangement for the *Thru* connection and the corresponding signal flow graph. Observe that we have made use of the fact that $S_{21} = S_{12}$ and that the error boxes are identical and symmetrically arranged. The signal flow graph can be easily reduced using the decomposition rules to give the measured scattering parameters at the measurement planes in terms of the scattering parameters of the error boxes as

$$T_{11} = \left. \frac{b_1}{a_1} \right|_{a_2=0} = S_{11} + \frac{S_{22}S_{12}^2}{1 - S_{22}^2} \quad (4.80a)$$

$$T_{12} = \left. \frac{b_1}{a_2} \right|_{a_1=0} = \frac{S_{12}^2}{1 - S_{22}^2} \quad (4.80b)$$

By symmetry we have $T_{22} = T_{11}$, and by reciprocity we have $T_{21} = T_{12}$.

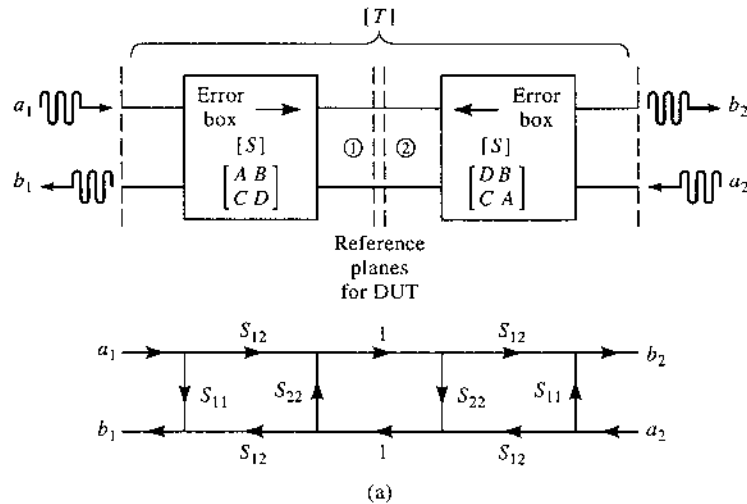


FIGURE 4.21a Block diagram and signal flow graph for the *Thru* connection.

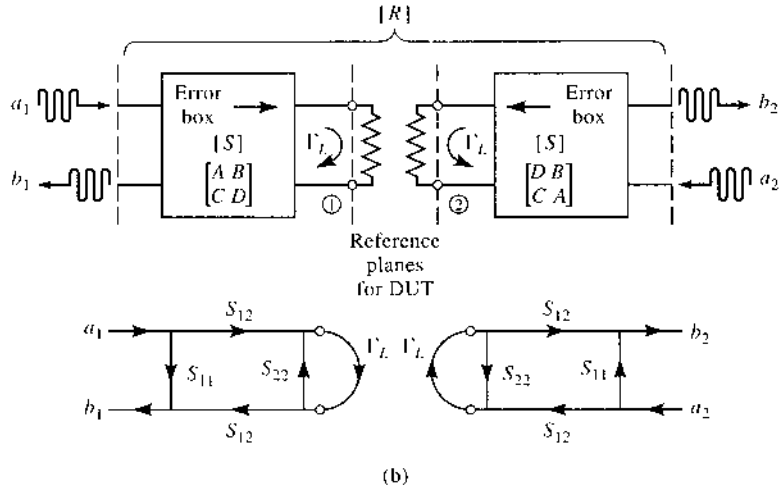


FIGURE 4.21b Block diagram and signal flow graph for the *Reflect* connection.

The *Reflect* connection is shown in Figure 4.21b, with the corresponding signal flow graph. Note that this arrangement effectively decouples the two measurement ports, so $R_{12} = R_{21} = 0$. The signal flow graph can be easily reduced to show that

$$R_{11} = \left. \frac{b_1}{a_1} \right|_{a_2=0} = S_{11} + \frac{S_{12}^2 \Gamma_L}{1 - S_{22} \Gamma_L}. \quad (4.81)$$

By symmetry we have $R_{22} = R_{11}$.

The *Line* connection is shown in Figure 4.21c, with its corresponding signal flow graph. A reduction similar to that used for the *Thru* case gives

$$L_{11} = \left. \frac{b_1}{a_1} \right|_{a_2=0} = S_{11} + \frac{S_{22} S_{12}^2 e^{-2\gamma \ell}}{1 - S_{22}^2 e^{-2\gamma \ell}}, \quad (4.82a)$$

$$L_{12} = \left. \frac{b_1}{a_2} \right|_{a_1=0} = \frac{S_{12}^2 e^{-\gamma \ell}}{1 - S_{22}^2 e^{-2\gamma \ell}}. \quad (4.82b)$$

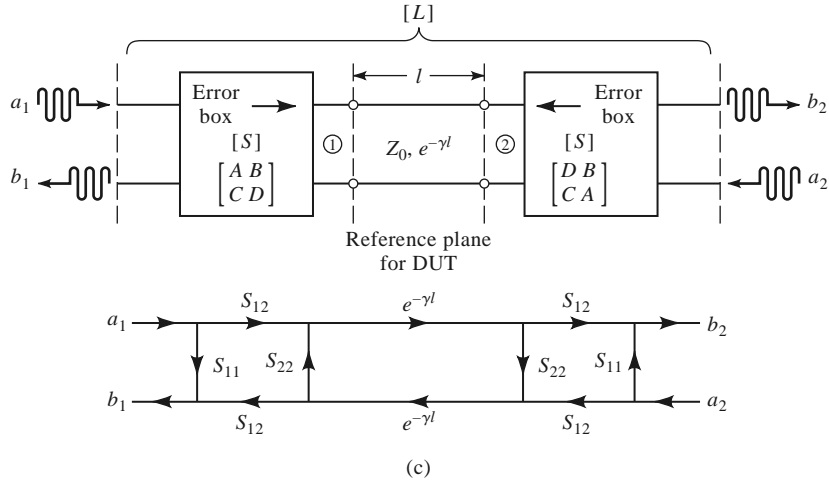


FIGURE 4.21c Block diagram and signal flow graph for the *Line* connection.

By symmetry and reciprocity we have $L_{22} = L_{11}$ and $L_{21} = L_{12}$.

We now have five equations (4.80)–(4.82) for the five unknowns S_{11} , S_{12} , S_{22} , Γ_L , and e^{γ^ℓ} ; the solution is straightforward but lengthy. Because (4.81) is the only equation that contains Γ_L , we can first solve the four equations in (4.80) and (4.82) for the other four unknowns. Equation (4.80b) can be used to eliminate S_{12} from (4.80a) and (4.82), and then S_{11} can be eliminated from (4.80a) and (4.82a). This leaves two equations for S_{22} and e^{γ^ℓ} :

$$L_{12}e^{2\gamma^\ell} - L_{12}S_{22}^2 = T_{12}e^{\gamma^\ell} - T_{12}S_{22}^2e^{\gamma^\ell}, \quad (4.83a)$$

$$e^{2\gamma^\ell}(T_{11} - S_{22}T_{12}) - T_{11}S_{22}^2 = L_{11}(e^{2\gamma^\ell} - S_{22}^2) - S_{22}T_{12}. \quad (4.83b)$$

Equation (4.83a) can be solved for S_{22} and substituted into (4.83b) to give a quadratic equation for e^{γ^ℓ} . Application of the quadratic formula then gives the solution for e^{γ^ℓ} in terms of the measured TRL scattering parameters as

$$e^{\gamma^\ell} = \frac{L_{12}^2 + T_{12}^2 - (T_{11} - L_{11})^2 \pm \sqrt{[L_{12}^2 + T_{12}^2 - (T_{11} - L_{11})^2]^2 - 4L_{12}^2T_{12}^2}}{2L_{12}T_{12}}. \quad (4.84)$$

The choice of sign can be determined by the requirement that the real and imaginary parts of γ be positive, or by knowing the phase of Γ_L [as determined from (4.83)] to within 180° .

Now multiply (4.80b) by S_{22} and subtract from (4.80a) to get

$$T_{11} = S_{11} + S_{22}T_{12}, \quad (4.85a)$$

and similarly multiply (4.82b) by $S_{22}e^{-\gamma^\ell}$ and subtract from (4.82a) to get

$$L_{11} = S_{11} + S_{22}L_{12}e^{-\gamma^\ell}. \quad (4.85b)$$

Eliminating S_{11} from these two equations gives S_{22} in terms of $e^{-\gamma^\ell}$ as

$$S_{22} = \frac{T_{11} - L_{11}}{T_{12} - L_{12}e^{-\gamma^\ell}}. \quad (4.86)$$

Solving (4.85a) for S_{11} gives

$$S_{11} = T_{11} - S_{22}T_{12}, \quad (4.87)$$

and solving (4.80b) for S_{12} gives

$$S_{12}^2 = T_{12}(1 - S_{22}^2). \quad (4.88)$$

Finally, (4.81) can be solved for Γ_L to give

$$\Gamma_L = \frac{R_{11} - S_{11}}{S_{12}^2 + S_{22}(R_{11} - S_{11})}. \quad (4.89)$$

Equations (4.84) and (4.86)–(4.89) give the scattering parameters for the error boxes, as well as the unknown reflection coefficient Γ_L (to within the sign), and the propagation factor $e^{-\gamma^\ell}$. This completes the calibration procedure for the TRL method.

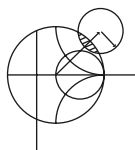
The scattering parameters of the DUT can now be measured at the measurement reference planes shown in Figure 4.20, and corrected using the above TRL error box parameters

to give the scattering parameters at the reference planes of the DUT. Because we are working with a cascade of three two-port networks, it is convenient to use $ABCD$ parameters. Thus, we convert the error box scattering parameters to the corresponding $ABCD$ parameters, and convert the measured scattering parameters of the cascade to the corresponding $A^m B^m C^m D^m$ parameters. If we use $A' B' C' D'$ to denote the parameters for the DUT, then we have

$$\begin{bmatrix} A^m & B^m \\ C^m & D^m \end{bmatrix} = \begin{bmatrix} A & B \\ C & D \end{bmatrix} \begin{bmatrix} A' & B' \\ C' & D' \end{bmatrix} \begin{bmatrix} D & B \\ C & A \end{bmatrix},$$

where the change in the elements of the last matrix account for the reversal of ports for the error box at port 2 of the DUT (see Problem 4.25). Then the $ABCD$ parameters for the DUT can be determined as

$$\begin{bmatrix} A' & B' \\ C' & D' \end{bmatrix} = \begin{bmatrix} A & B \\ C & D \end{bmatrix}^{-1} \begin{bmatrix} A^m & B^m \\ C^m & D^m \end{bmatrix} \begin{bmatrix} D & B \\ C & A \end{bmatrix}^{-1}. \quad (4.90)$$



POINT OF INTEREST: Computer-Aided Design for Microwave Circuits

Computer-aided design (CAD) software packages have become essential tools for the analysis, design, and optimization of RF and microwave circuits and systems. Several microwave CAD products are commercially available, including Microwave Office (Applied Wave Research), ADS (Agilent Technologies), Microwave Studio (CST), Designer (Ansoft), and many others. RF and microwave CAD packages can be divided into two types: those that use “physics-based” solutions, where Maxwell’s equations are numerically solved for physical geometries such as printed circuit geometries or waveguides, and “circuit-based” solutions, which use equivalent circuits for various elements, including distributed elements, discontinuities, coupled lines, and active devices. Some packages combine these two approaches. Both linear and nonlinear modeling, as well as circuit optimization, are generally possible. Although such computer programs can be fast, powerful, and accurate, they cannot serve as a substitute for engineering experience and a good understanding of microwave principles.

A typical design process usually begins with specifications or design goals for the circuit or system. Based on previous designs and his or her experience, an engineer can develop an initial design, including specific components and a circuit layout. CAD can then be used to model and analyze the design, using data for each of the components and including effects such as loss and discontinuities. The software can be used to optimize the design by adjusting some of the circuit parameters to achieve the best performance. If the specifications are not met, the design may have to be revised. CAD tools can also be used to study the effects of component tolerances and errors to improve circuit reliability and robustness. When the design meets the specifications, an engineering prototype can be built and tested. If the measured results satisfy the specifications, the design process is completed. Otherwise the design will need to be revised and the procedure repeated.

Without CAD tools the design process would require the construction and measurement of laboratory prototypes at each iteration, which is expensive and time consuming. Thus, CAD can greatly decrease the time and cost of a design while enhancing its quality. The simulation and optimization process is especially important for monolithic microwave integrated circuits because these circuits cannot easily be tuned or trimmed after fabrication.

CAD techniques are not without limitations, however. Of primary importance is the fact that any computer model is only an approximation to a “real-world” physical circuit and cannot completely account for the inevitable differences due to component and fabrication tolerances, surface roughness, spurious coupling, higher order modes, junction discontinuities, thermal effects, and a number of other practical issues that can occur with a physical circuit or device.

4.6

DISCONTINUITIES AND MODAL ANALYSIS

By either necessity or design, microwave circuits and networks often consist of transmission lines with various types of discontinuities. In some cases discontinuities are an unavoidable result of mechanical or electrical transitions from one medium to another (e.g., a junction between two waveguides, or a coax-to-microstrip transition), and the discontinuity effect is unwanted but may be significant enough to warrant characterization. In other cases discontinuities may be deliberately introduced into the circuit to perform a certain electrical function (e.g., reactive diaphragms in waveguide, or stubs on a microstrip line for matching or filter circuits). In any event, a transmission line discontinuity can be represented as an equivalent circuit at some point on the transmission line. Depending on the type of discontinuity, the equivalent circuit may be a simple shunt or series element across the line or, in the more general case, a T- or π -equivalent circuit may be required. The component values of an equivalent circuit depend on the parameters of the line and the discontinuity, as well as on the frequency of operation. In some cases the equivalent circuit involves a shift in the phase reference planes on the transmission lines. Once the equivalent circuit of a given discontinuity is known, its effect can be incorporated into the analysis or design of the network using the theory developed previously in this chapter.

The purpose of the present section is to discuss how equivalent circuits are obtained for transmission line discontinuities; we will see that one approach is to start with a field theory solution to a canonical discontinuity problem and develop a circuit model with component values. This is thus another example of our objective of replacing complicated field analyses with circuit concepts. In other cases, it may be easier to measure the network parameters of an isolated discontinuity.

Figures 4.22 and 4.23 show some common transmission line discontinuities and their equivalent circuits. As shown in Figures 4.22a–4.22c, thin metallic diaphragms (or “irises”) can be placed in the cross section of a waveguide to yield equivalent shunt inductance, capacitance, or a resonant combination. Similar effects occur with step changes in the height or width of the waveguide, as shown in Figures 4.22d and 4.22e. Similar discontinuities can also be made in circular waveguide. The classic reference for waveguide discontinuities and their equivalent circuits is the *Waveguide Handbook* [8].

Some typical microstrip discontinuities and transitions are shown in Figure 4.23; similar geometries exist for stripline and other printed transmission lines such as slotline, covered microstrip, coplanar waveguide, etc. Although approximate equivalent circuits have been developed for some printed transmission line discontinuities [9], many do not lend themselves to easy or accurate modeling, and must be treated by numerical analysis. Modern CAD tools are usually capable of accurately modeling such problems.

Modal Analysis of an H -Plane Step in Rectangular Waveguide

The field analysis of most transmission line discontinuity problems is difficult, and beyond the scope of this book. The technique of waveguide *modal analysis*, however, is relatively straightforward and similar in principle to the reflection/transmission problems that were discussed in Chapters 1 and 2. In addition, modal analysis is a rigorous and versatile technique that can be applied to a number of waveguide and coax discontinuity problems, and lends itself well to computer implementation. We will illustrate the technique by applying it to the problem of finding the equivalent circuit of an H -plane step (change in width) in a rectangular waveguide.

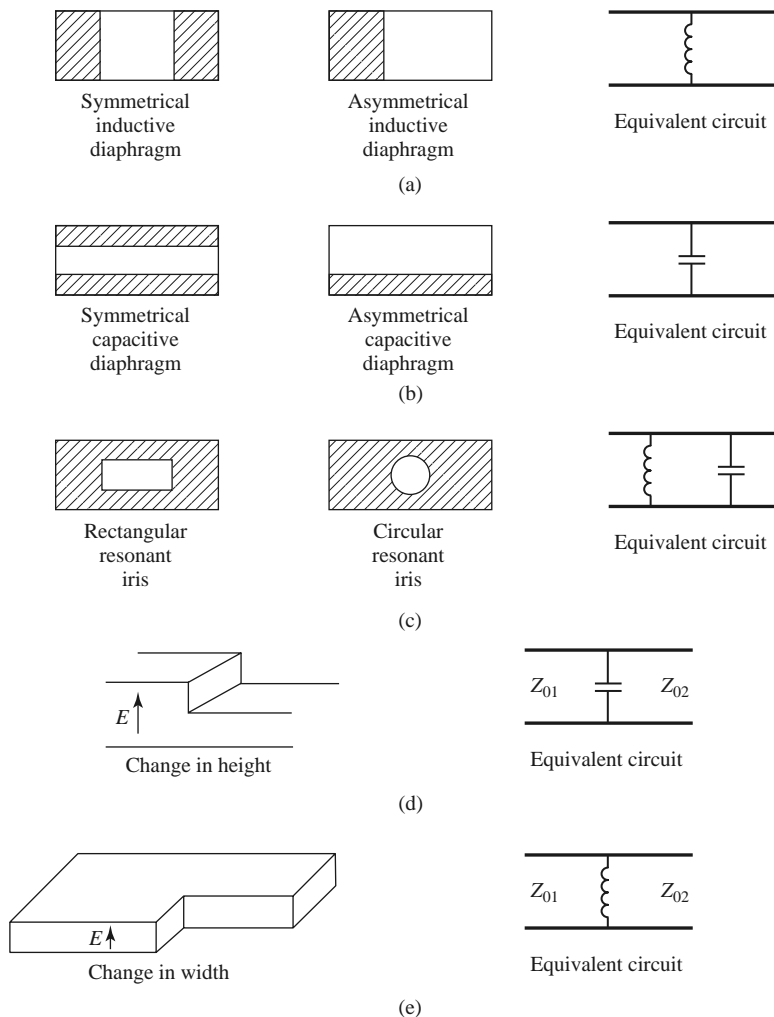


FIGURE 4.22 Rectangular waveguide discontinuities.

The geometry of the H -plane waveguide step is shown in Figure 4.24. It is assumed that only the dominant TE_{10} mode is propagating in guide 1 ($z < 0$) and is incident on the junction from $z < 0$. It is also assumed that no modes are propagating in guide 2, although the analysis to follow is still valid if propagation can occur in guide 2. From Section 3.3, the transverse components of the incident TE_{10} mode can be written, for $z < 0$, as

$$E_y^i = \sin \frac{\pi x}{a} e^{-j\beta_1^a z}, \quad (4.91a)$$

$$H_x^i = \frac{-1}{Z_1^a} \sin \frac{\pi x}{a} e^{-j\beta_1^a z}, \quad (4.91b)$$

where

$$\beta_n^a = \sqrt{k_0^2 - \left(\frac{n\pi}{a}\right)^2} \quad (4.92)$$

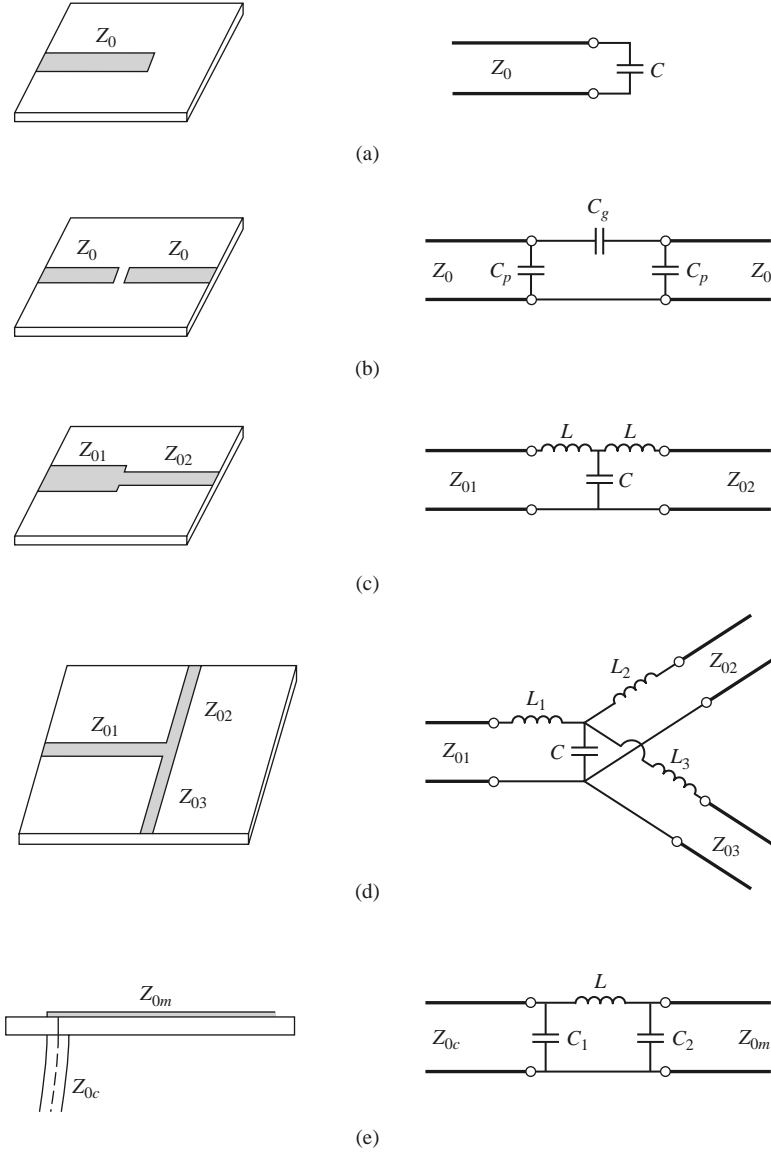


FIGURE 4.23 Some common microstrip discontinuities. (a) Open-ended microstrip. (b) Gap in microstrip. (c) Change in width. (d) T-junction. (e) Coax-to-microstrip junction.

is the propagation constant of the TE_{n0} mode in guide 1 (of width a), and

$$Z_n^a = \frac{k_0 \eta_0}{\beta_n^a} \quad (4.93)$$

is the wave impedance of the TE_{n0} mode in guide 1. Because of the discontinuity at $z = 0$ there will be reflected and transmitted waves in both guides, consisting of infinite sets of TE_{n0} modes in guides 1 and 2. Only the TE_{10} mode will propagate in guide 1, but higher order modes are also important in this problem because they account for stored energy,

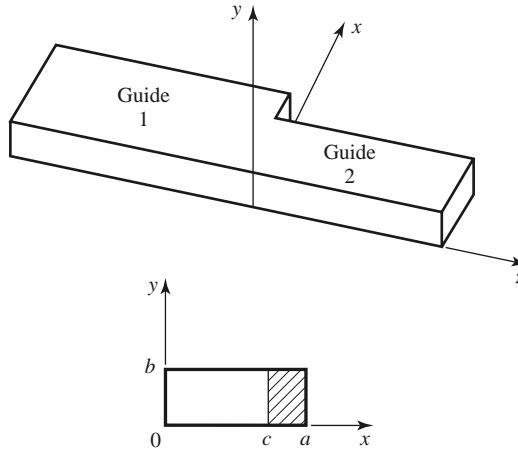


FIGURE 4.24 Geometry of an H -plane step (change in width) in a rectangular waveguide.

localized near $z = 0$. Because there is no y variation introduced by this discontinuity, TE_{nm} modes for $m \neq 0$ are not excited, nor are any TM modes. A more general discontinuity, however, may excite such modes.

The reflected modes in guide 1 may be written, for $z < 0$, as

$$E_y^r = \sum_{n=1}^{\infty} A_n \sin \frac{n\pi x}{a} e^{j\beta_n^a z}, \quad (4.94a)$$

$$H_x^r = \sum_{n=1}^{\infty} \frac{A_n}{Z_n^a} \sin \frac{n\pi x}{a} e^{j\beta_n^a z}, \quad (4.94b)$$

where A_n is the unknown amplitude coefficient of the reflected TE_{n0} mode in guide 1. The reflection coefficient of the incident TE_{10} mode is then A_1 . Similarly, the transmitted modes into guide 2 can be written, for $z > 0$, as

$$E_y^t = \sum_{n=1}^{\infty} B_n \sin \frac{n\pi x}{c} e^{-j\beta_n^c z}, \quad (4.95a)$$

$$H_x^t = - \sum_{n=1}^{\infty} \frac{B_n}{Z_n^c} \sin \frac{n\pi x}{c} e^{-j\beta_n^c z}, \quad (4.95b)$$

where the propagation constant in guide 2 is

$$\beta_n^c = \sqrt{k_0^2 - \left(\frac{n\pi}{c}\right)^2}, \quad (4.96)$$

and the wave impedance in guide 2 is

$$Z_n^c = \frac{k_0 \eta_0}{\beta_n^c}. \quad (4.97)$$

At $z = 0$, the transverse fields (E_y , H_x) must be continuous for $0 < x < c$; in addition, E_y must be zero for $c < x < a$ because of the step. Enforcing these boundary conditions leads to the following equations:

$$E_y = \sin \frac{\pi x}{a} + \sum_{n=1}^{\infty} A_n \sin \frac{n\pi x}{a} = \begin{cases} \sum_{n=1}^{\infty} B_n \sin \frac{n\pi x}{c} & \text{for } 0 < x < c, \\ 0 & \text{for } c < x < a, \end{cases} \quad (4.98a)$$

$$H_x = \frac{-1}{Z_1^a} \sin \frac{\pi x}{a} + \sum_{n=1}^{\infty} \frac{A_n}{Z_n^a} \sin \frac{n\pi x}{a} = - \sum_{n=1}^{\infty} \frac{B_n}{Z_n^c} \sin \frac{n\pi x}{c} \text{ for } 0 < x < c. \quad (4.98b)$$

Equations (4.98a) and (4.98b) constitute a doubly infinite set of linear equations for the modal coefficients A_n and B_n . We will first eliminate the B_n and then truncate the resulting equation to a finite number of terms and solve for the A_n .

Multiplying (4.98a) by $\sin(m\pi x/a)$, integrating from $x = 0$ to a , and using the orthogonality relations from Appendix D yields

$$\frac{a}{2} \delta_{m1} + \frac{a}{2} A_m = \sum_{n=1}^{\infty} B_n I_{mn} = \sum_{k=1}^{\infty} B_k I_{mk}, \quad (4.99)$$

where

$$I_{mn} = \int_{x=0}^c \sin \frac{m\pi x}{a} \sin \frac{n\pi x}{c} dx \quad (4.100)$$

is an integral that can be easily evaluated, and

$$\delta_{mn} = \begin{cases} 1 & \text{if } m = n \\ 0 & \text{if } m \neq n \end{cases} \quad (4.101)$$

is the Kronecker delta symbol. Now solve (4.98b) for B_k by multiplying (4.98b) by $\sin(k\pi x/c)$ and integrating from $x = 0$ to c . After using orthogonality relations, we obtain

$$\frac{-1}{Z_1^a} I_{k1} + \sum_{n=1}^{\infty} \frac{A_n}{Z_n^a} I_{kn} = \frac{-c B_k}{2 Z_k^c}. \quad (4.102)$$

Substituting B_k from (4.102) into (4.99) gives an infinite set of linear equations for the A_n , where $m = 1, 2, \dots$,

$$\frac{a}{2} A_m + \sum_{n=1}^{\infty} \sum_{k=1}^{\infty} \frac{2 Z_k^c I_{mk} I_{kn} A_n}{c Z_n^a} = \sum_{k=1}^{\infty} \frac{2 Z_k^c I_{mk} I_{k1}}{c Z_1^a} - \frac{a}{2} \delta_{m1}. \quad (4.103)$$

For numerical calculation we can truncate these summations to N terms, which will result in N linear equations for the first N coefficients, A_n . For example, let $N = 1$. Then (4.103) reduces to

$$\frac{a}{2} A_1 + \frac{2 Z_1^c I_{11}^2}{c Z_1^a} A_1 = \frac{2 Z_1^c I_{11}^2}{c Z_1^a} - \frac{a}{2}. \quad (4.104)$$

Solving for A_1 (the reflection coefficient of the incident TE₁₀ mode) gives

$$A_1 = \frac{Z_\ell - Z_1^a}{Z_\ell + Z_1^a} \text{ for } N = 1, \quad (4.105)$$

where $Z_\ell = 4Z_1^c I_{11}^2 / ac$, which looks like an effective load impedance to guide 1. Accuracy is improved by using larger values of N and leads to a set of equations that can be written in matrix form as

$$[Q][A] = [P], \quad (4.106)$$

where $[Q]$ is a square $N \times N$ matrix of coefficients,

$$Q_{mn} = \frac{a}{2} \delta_{mn} + \sum_{k=1}^N \frac{2Z_k^c I_{mk} I_{kn}}{cZ_n^a}, \quad (4.107)$$

$[P]$ is an $N \times 1$ column vector of coefficients given by

$$P_m = \sum_{k=1}^N \frac{2Z_k^c I_{mk} I_{k1}}{cZ_1^a} - \frac{a}{2} \delta_{m1}, \quad (4.108)$$

and $[A]$ is an $N \times 1$ column vector of the coefficients A_n . After the A_n are found, the B_n can be calculated from (4.102), if desired. Equations (4.106)–(4.108) lend themselves well to computer implementation, and Figure 4.25 shows the results of such a calculation for various matrix sizes.

If the width c of guide 2 is such that all modes are cut off (evanescent), then no real power can be transmitted into guide 2, and all the incident power is reflected back into guide 1. The evanescent fields on both sides of the discontinuity store reactive power, however, which implies that the step discontinuity and guide 2 beyond the discontinuity look like a reactance (in this case an inductive reactance) to an incident TE_{10} mode in guide 1. Thus the equivalent circuit of the H -plane step looks like a shunt inductor at the $z = 0$ plane of guide 1, as shown in Figure 4.22e. The equivalent reactance can be found from the reflection coefficient A_1 [after solving (4.106)] as

$$X = -jZ_1^a \frac{1 + A_1}{1 - A_1}. \quad (4.109)$$

Figure 4.25 shows the normalized equivalent inductance versus the ratio of the guide widths c/a for a free-space wavelength $\lambda = 1.4a$ and for $N = 1, 2$, and 10 equations. The

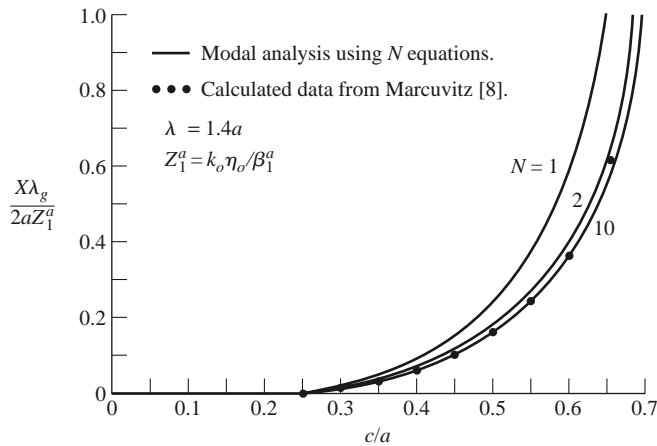


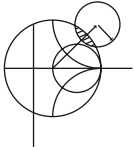
FIGURE 4.25 Equivalent inductance of an H -plane asymmetric step.

modal analysis results are compared to data from reference [8]. Note that the solution converges very quickly (because of the fast exponential decay of the higher order evanescent modes), and that the result using just two modes is very close to the data of reference [8].

The fact that the H -plane step appears inductive is a result of the actual value of the reflection coefficient, A_1 , but we can verify the inductive nature of the discontinuity by computing the complex power flow into the evanescent modes on either side of the discontinuity. For example, the complex power flow into guide 2 can be found as

$$\begin{aligned}
 P &= \int_{x=0}^c \int_{y=0}^b \bar{\mathbf{E}} \times \bar{\mathbf{H}}^* \Big|_{z=0^+} \cdot \hat{\mathbf{z}} dx dy \\
 &= -b \int_{x=0}^c E_y H_x^* dx \\
 &= -b \int_{x=0}^c \left[\sum_{n=1}^{\infty} B_n \sin \frac{n\pi x}{c} \right] \left[- \sum_{m=1}^{\infty} \frac{B_m^*}{Z_m^{c*}} \sin \frac{m\pi x}{c} \right] dx \\
 &= \frac{bc}{2} \sum_{n=1}^{\infty} \frac{|B_n|^2}{Z_n^{c*}} \\
 &= \frac{jbc}{2k_0\eta_0} \sum_{n=1}^{\infty} |B_n|^2 |\beta_n^c|,
 \end{aligned} \tag{4.110}$$

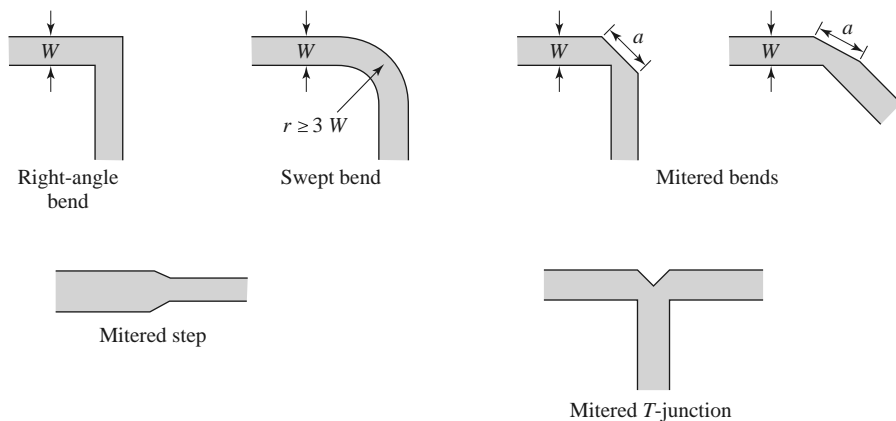
where the orthogonality property of the sine functions was used, as well as (4.95)–(4.97). Equation (4.110) shows that the complex power flow into guide 2 is positive imaginary, implying stored magnetic energy and an inductive reactance. A similar result can be derived for the evanescent modes in guide 1; this is left as a problem.



POINT OF INTEREST: Microstrip Discontinuity Compensation

Because a microstrip circuit is easy to fabricate and allows the convenient integration of passive and active components, many types of microwave circuits and subsystems are made in microstrip form. One problem with microstrip circuits (and other planar circuits) is that the inevitable discontinuities at bends, step changes in widths, and junctions can cause degradation in circuit performance. This is because such discontinuities introduce parasitic reactances that can lead to phase and amplitude errors, input and output mismatch, and possibly spurious coupling or radiation. One approach for eliminating such effects is to construct an equivalent circuit for the discontinuity (perhaps by measurement), including it in the design of the circuit, and compensating for its effect by adjusting other circuit parameters (such as line lengths and characteristic impedances, or tuning stubs). Another approach is to minimize the effect of a discontinuity by compensating the discontinuity directly, often by chamfering or mitering the conductor.

Consider the case of a bend in a microstrip line. The straightforward right-angle bend shown below has a parasitic discontinuity capacitance caused by the increased conductor area at the corner of the bend. This effect could be eliminated by making a smooth, “swept” bend with a radius $r \geq 3W$, but this takes up more space. Alternatively, the right-angle bend can be compensated by mitering the corner, which has the effect of reducing the excess capacitance at the bend. As shown later, this technique can be applied to bends of arbitrary angle. The optimum value of the miter length, a , depends on the characteristic impedance and the bend angle, but a value of $a = 1.8W$ is often used in practice. The technique of mitering can also be used to compensate step and T-junction discontinuities, as shown on the next page.



Reference: T. C. Edwards, *Foundations for Microwave Circuit Design*, John Wiley & Sons, New York, 1981.

4.7

EXCITATION OF WAVEGUIDES—ELECTRIC AND MAGNETIC CURRENTS

So far we have considered the propagation, reflection, and transmission of guided waves in the absence of sources, but obviously the waveguide or transmission line must be coupled to a generator or some other source of power. For TEM or quasi-TEM lines, there is usually only one propagating mode that can be excited by a given source, although there may be reactance (stored energy) associated with a given feed. In the waveguide case, it may be possible for several propagating modes to be excited, along with evanescent modes that store energy. In this section we will develop a formalism for determining the excitation of a given waveguide mode due to an arbitrary electric or magnetic current source. This theory can then be used to find the excitation and input impedance of probe and loop feeds and, in the next section, to determine the excitation of waveguides by apertures.

Current Sheets That Excite Only One Waveguide Mode

Consider an infinitely long rectangular waveguide with a transverse sheet of electric surface current density at $z = 0$, as shown in Figure 4.26. First assume that this current has \hat{x} and \hat{y} components given as

$$\bar{J}_s^{\text{TE}}(x, y) = -\hat{x} \frac{2A_{mn}^+ n\pi}{b} \cos \frac{m\pi x}{a} \sin \frac{n\pi y}{b} + \hat{y} \frac{2A_{mn}^+ m\pi}{a} \sin \frac{m\pi x}{a} \cos \frac{n\pi y}{b}. \quad (4.111)$$

We will show that such a current excites a single TE_{mn} waveguide mode traveling away from the current source in both the $+z$ and $-z$ directions.

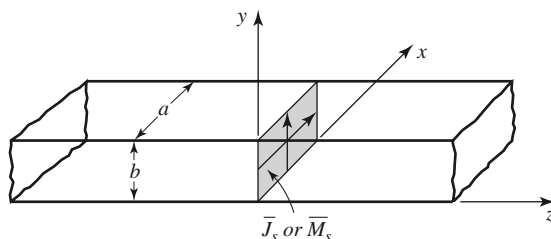


FIGURE 4.26 An infinitely long rectangular waveguide with surface current densities at $z = 0$.

From Table 3.2, the transverse fields for positive and negative traveling TE_{mn} waveguide modes can be written as

$$E_x^\pm = Z_{TE} \left(\frac{n\pi}{b} \right) A_{mn}^\pm \cos \frac{m\pi x}{a} \sin \frac{n\pi y}{b} e^{\mp j\beta z}, \quad (4.112a)$$

$$E_y^\pm = -Z_{TE} \left(\frac{m\pi}{a} \right) A_{mn}^\pm \sin \frac{m\pi x}{a} \cos \frac{n\pi y}{b} e^{\mp j\beta z}, \quad (4.112b)$$

$$H_x^\pm = \pm \left(\frac{m\pi}{a} \right) A_{mn}^\pm \sin \frac{m\pi x}{a} \cos \frac{n\pi y}{b} e^{\mp j\beta z}, \quad (4.112c)$$

$$H_y^\pm = \pm \left(\frac{n\pi}{b} \right) A_{mn}^\pm \cos \frac{m\pi x}{a} \sin \frac{n\pi y}{b} e^{\mp j\beta z}, \quad (4.112d)$$

where the \pm notation refers to waves traveling in the $+z$ direction or $-z$ direction with amplitude coefficients A_{mn}^+ and A_{mn}^- , respectively.

From (1.36) and (1.37), the following boundary conditions must be satisfied at $z = 0$:

$$(\bar{E}^+ - \bar{E}^-) \times \hat{z} = 0, \quad (4.113a)$$

$$\hat{z} \times (\bar{H}^+ - \bar{H}^-) = \bar{J}_s. \quad (4.113b)$$

Equation (4.112a) states that the transverse components of the electric field must be continuous at $z = 0$, which when applied to (4.112a) and (4.112b), gives

$$A_{mn}^+ = A_{mn}^-. \quad (4.114)$$

Equation (4.113b) states that the discontinuity in the transverse magnetic field is equal to the electric surface current density. Thus, the surface current density at $z = 0$ must be

$$\begin{aligned} \bar{J}_s &= \hat{y}(H_x^+ - H_x^-) - \hat{x}(H_y^+ - H_y^-) \\ &= -\hat{x} \frac{2A_{mn}^+ n\pi}{b} \cos \frac{m\pi x}{a} \sin \frac{n\pi y}{b} + \hat{y} \frac{2A_{mn}^+ m\pi}{a} \sin \frac{m\pi x}{a} \cos \frac{n\pi y}{b}, \end{aligned} \quad (4.115)$$

where (4.114) was used. This current is seen to be the same as the current of (4.111), which shows, by the uniqueness theorem, that such a current will excite only the TE_{mn} mode propagating in each direction, since Maxwell's equations and all boundary conditions are satisfied.

The analogous electric current that excites only the TM_{mn} mode can be shown to be

$$\bar{J}_s^{\text{TM}}(x, y) = \hat{x} \frac{2B_{mn}^+ m\pi}{a} \cos \frac{m\pi x}{a} \sin \frac{n\pi y}{b} + \hat{y} \frac{2B_{mn}^+ n\pi}{b} \sin \frac{m\pi x}{a} \cos \frac{n\pi y}{b}. \quad (4.116)$$

It is left as a problem to verify that this current excites TM_{mn} modes that satisfy the appropriate boundary conditions.

Similar results can be derived for magnetic surface current sheets. From (1.36) and (1.37) the appropriate boundary conditions are

$$(\bar{E}^+ - \bar{E}^-) \times \hat{z} = \bar{M}_s, \quad (4.117a)$$

$$\hat{z} \times (\bar{H}^+ - \bar{H}^-) = 0. \quad (4.117b)$$

For a magnetic current sheet at $z = 0$, the TE_{mn} waveguide mode fields of (4.112) must now have continuous H_x and H_y field components, due to (4.117b). This results in the condition that

$$A_{mn}^+ = -A_{mn}^-. \quad (4.118)$$

Then applying (4.117a) gives the source current as

$$\bar{M}_s^{\text{TE}} = \frac{-\hat{x}2Z_{\text{TE}}A_{mn}^+m\pi}{a} \sin \frac{m\pi x}{a} \cos \frac{n\pi y}{b} - \hat{y} \frac{2Z_{\text{TE}}A_{mn}^+n\pi}{b} \cos \frac{m\pi x}{a} \sin \frac{n\pi y}{b}. \quad (4.119)$$

The corresponding magnetic surface current that excites only the TM_{mn} mode can be shown to be

$$\bar{M}_s^{\text{TM}} = \frac{-\hat{x}2B_{mn}^+n\pi}{b} \sin \frac{m\pi x}{a} \cos \frac{n\pi y}{b} + \frac{\hat{y}2B_{mn}^+m\pi}{a} \cos \frac{m\pi x}{a} \sin \frac{n\pi y}{b}. \quad (4.120)$$

These results show that a single waveguide mode can be selectively excited, to the exclusion of all other modes, by either an electric or magnetic current sheet of the appropriate form. In practice, however, such currents are difficult to generate and are usually only approximated with one or two probes or loops. In this case many modes may be excited, but usually most of these modes are evanescent.

Mode Excitation from an Arbitrary Electric or Magnetic Current Source

We now consider the excitation of waveguide modes by an arbitrary electric or magnetic current source [4]. With reference to Figure 4.27, first consider an electric current source \bar{J} located between two transverse planes at z_1 and z_2 , which generates the fields \bar{E}^+ , \bar{H}^+ traveling in the $+z$ direction, and the fields \bar{E}^- , \bar{H}^- traveling in the $-z$ direction. These fields can be expressed in terms of the waveguide modes as follows:

$$\bar{E}^+ = \sum_n A_n^+ \bar{E}_n^+ = \sum_n A_n^+ (\bar{e}_n + \hat{z}e_{zn})e^{-j\beta_n z}, \quad z > z_2, \quad (4.121a)$$

$$\bar{H}^+ = \sum_n A_n^+ \bar{H}_n^+ = \sum_n A_n^+ (\bar{h}_n + \hat{z}h_{zn})e^{-j\beta_n z}, \quad z > z_2, \quad (4.121b)$$

$$\bar{E}^- = \sum_n A_n^- \bar{E}_n^- = \sum_n A_n^- (\bar{e}_n - \hat{z}e_{zn})e^{j\beta_n z}, \quad z < z_1, \quad (4.121c)$$

$$\bar{H}^- = \sum_n A_n^- \bar{H}_n^- = \sum_n A_n^- (-\bar{h}_n + \hat{z}h_{zn})e^{j\beta_n z}, \quad z < z_1, \quad (4.121d)$$

where the single index n is used to represent any possible TE or TM mode. For a given current \bar{J} , we can determine the unknown amplitude A_n^+ by using the Lorentz reciprocity theorem of (1.155) with $\bar{M}_1 = \bar{M}_2 = 0$ (since here we are only considering an electric current source),

$$\oint_S (\bar{E}_1 \times \bar{H}_2 - \bar{E}_2 \times \bar{H}_1) \cdot d\bar{s} = \int_V (\bar{E}_2 \cdot \bar{J}_1 - \bar{E}_1 \cdot \bar{J}_2) dv,$$

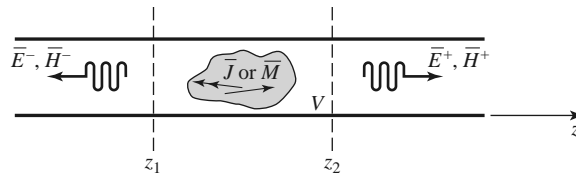


FIGURE 4.27 An arbitrary electric or magnetic current source in an infinitely long waveguide.

where S is a closed surface enclosing the volume V , and \bar{E}_i, \bar{H}_i are the fields due to the current source \bar{J}_i (for $i = 1$ or 2).

To apply the reciprocity theorem to the present problem we let the volume V be the region between the waveguide walls and the transverse cross-section planes at z_1 and z_2 . Then let $\bar{E}_1 = \bar{E}^\pm$ and $\bar{H}_1 = \bar{H}^\pm$, depending on whether $z \geq z_2$ or $z \leq z_1$, and let \bar{E}_2, \bar{H}_2 be the n th waveguide mode traveling in the negative z direction:

$$\begin{aligned}\bar{E}_2 &= \bar{E}_n^- = (\bar{e}_n - \hat{z}e_{zn})e^{j\beta_n z}, \\ \bar{H}_2 &= \bar{H}_n^- = (-\bar{h}_n + \hat{z}h_{zn})e^{j\beta_n z}.\end{aligned}$$

Substitution into the above form of the reciprocity theorem gives, with $\bar{J}_1 = \bar{J}$ and $\bar{J}_2 = 0$,

$$\oint_S (\bar{E}^\pm \times \bar{H}_n^- - \bar{E}_n^- \times \bar{H}^\pm) \cdot d\bar{s} = \int_V \bar{E}_n^- \cdot \bar{J} dv. \quad (4.122)$$

The portion of the surface integral over the waveguide walls vanishes because the tangential electric field is zero there; that is, $\bar{E} \times \bar{H} \cdot \hat{z} = \bar{H} \cdot (\hat{z} \times \bar{E}) = 0$ on the waveguide walls. This reduces the integration to the guide cross section, S_0 , at the planes z_1 and z_2 . In addition, the waveguide modes are orthogonal over the guide cross section:

$$\begin{aligned}\int_{S_0} \bar{E}_m^\pm \times \bar{H}_n^\pm \cdot d\bar{s} &= \int_{S_0} (\bar{e}_m \pm \hat{z}e_{zm}) \times (\pm \bar{h}_n + \hat{z}h_{zn}) \cdot \hat{z} ds \\ &= \pm \int_{S_0} \bar{e}_m \times \bar{h}_n \cdot \hat{z} ds = 0, \text{ for } m \neq n.\end{aligned} \quad (4.123)$$

Using (4.121) and (4.123) then reduces (4.122) to

$$\begin{aligned}A_n^+ \int_{z_2} (\bar{E}_n^+ \times \bar{H}_n^- - \bar{E}_n^- \times \bar{H}_n^+) \cdot d\bar{s} + A_n^- \int_{z_1} (\bar{E}_n^- \times \bar{H}_n^- - \bar{E}_n^- \times \bar{H}_n^-) \cdot d\bar{s} \\ = \int_V \bar{E}_n^- \cdot \bar{J} dv.\end{aligned}$$

Because the second integral vanishes, this further reduces to

$$\begin{aligned}A_n^+ \int_{z_2} [(\bar{e}_n + \hat{z}e_{zn}) \times (-\bar{h}_n + \hat{z}h_{zn}) - (\bar{e}_n - \hat{z}e_{zn}) \times (\bar{h}_n + \hat{z}h_{zn})] \cdot \hat{z} ds \\ = -2A_n^+ \int_{z_2} \bar{e}_n \times \bar{h}_n \cdot \hat{z} ds = \int_V \bar{E}_n^- \cdot \bar{J} dv,\end{aligned}$$

or

$$A_n^+ = \frac{-1}{P_n} \int_V \bar{E}_n^- \cdot \bar{J} dv = \frac{-1}{P_n} \int_V (\bar{e}_n - \hat{z}e_{zn}) \cdot \bar{J} e^{j\beta_n z} dv, \quad (4.124)$$

where

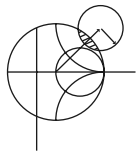
$$P_n = 2 \int_{S_0} \bar{e}_n \times \bar{h}_n \cdot \hat{z} ds \quad (4.125)$$

is a normalization constant proportional to the power flow of the n th mode.

By repeating the above procedure with $\bar{E}_2 = \bar{E}_n^+$ and $\bar{H}_2 = \bar{H}_n^+$, we can derive the amplitude of the negatively traveling waves as

$$A_n^- = \frac{-1}{P_n} \int_V \bar{E}_n^+ \cdot \bar{J} dv = \frac{-1}{P_n} \int_V (\bar{e}_n + \hat{z}e_{zn}) \cdot \bar{J} e^{-j\beta_n z} dv. \quad (4.126)$$

These results are quite general, being applicable to any type of waveguide (including planar lines such as stripline and microstrip), where modal fields can be defined. Example 4.8 applies this theory to the problem of a probe-fed rectangular waveguide.



EXAMPLE 4.8 PROBE-FED RECTANGULAR WAVEGUIDE

For the probe-fed rectangular waveguide shown in Figure 4.28, determine the amplitudes of the forward and backward traveling TE_{10} modes, and the input resistance seen by the probe. Assume that the TE_{10} mode is the only propagating mode.

Solution

If the current probe is assumed to have an infinitesimal diameter, the source volume current density \bar{J} can be written as

$$\bar{J}(x, y, z) = I_0 \delta\left(x - \frac{a}{2}\right) \delta(z) \hat{y} \text{ for } 0 \leq y \leq b.$$

From Chapter 3 the TE_{10} modal fields can be written as

$$\begin{aligned} \bar{e}_1 &= \hat{y} \sin \frac{\pi x}{a}, \\ \bar{h}_1 &= \frac{-\hat{x}}{Z_1} \sin \frac{\pi x}{a}, \end{aligned}$$

where $Z_1 = k_0 \eta_0 / \beta_1$ is the TE_{10} wave impedance. From (4.125) the normalization constant P_1 is

$$P_1 = \frac{2}{Z_1} \int_{x=0}^a \int_{y=0}^b \sin^2 \frac{\pi x}{a} dx dy = \frac{ab}{Z_1}.$$

Then from (4.124) the amplitude A_1^+ is

$$A_1^+ = \frac{-1}{P_1} \int_V \sin \frac{\pi x}{a} e^{j\beta_1 z} I_0 \delta\left(x - \frac{a}{2}\right) \delta(z) dx dy dz = \frac{-I_0 b}{P_1} = \frac{-Z_1 I_0}{a}.$$

Similarly,

$$A_1^- = \frac{-Z_1 I_0}{a}.$$

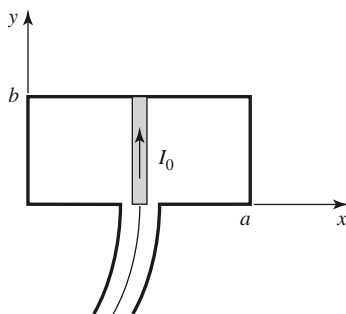


FIGURE 4.28 A uniform current probe in a rectangular waveguide.

If the TE_{10} mode is the only propagating mode in the waveguide, then this mode carries all of the average power, which can be calculated for real Z_1 as

$$\begin{aligned}
 P &= \frac{1}{2} \int_{S_0} \bar{E}^+ \times \bar{H}^{+*} \cdot d\bar{s} + \frac{1}{2} \int_{S_0} \bar{E}^- \times \bar{H}^{-*} \cdot d\bar{s} \\
 &= \int_{S_0} \bar{E}^+ \times \bar{H}^{+*} \cdot d\bar{s} \\
 &= \int_{x=0}^a \int_{y=0}^b \frac{|A_1^+|^2}{Z_1} \sin^2 \frac{\pi x}{a} dx dy \\
 &= \frac{ab|A_1^+|^2}{2Z_1}.
 \end{aligned}$$

If the input resistance seen looking into the probe is R_{in} , and the terminal current is I_0 , then $P = I_0^2 R_{in}/2$, so that the input resistance is

$$R_{in} = \frac{2P}{I_0^2} = \frac{ab|A_1^+|^2}{I_0^2 Z_1} = \frac{bZ_1}{a},$$

which is real for real Z_1 (corresponding to a propagating TE_{10} mode). ■

A similar derivation can be carried out for a magnetic current source \bar{M} (e.g., a small loop). This source will also generate positively and negatively traveling waves, which can be expressed as a superposition of waveguide modes, as in (4.121). For $\bar{J}_1 = \bar{J}_2 = 0$, the reciprocity theorem of (1.155) reduces to

$$\oint_S (\bar{E}_1 \times \bar{H}_2 - \bar{E}_2 \times \bar{H}_1) \cdot d\bar{s} = \int_V (\bar{H}_1 \cdot \bar{M}_2 - \bar{H}_2 \cdot \bar{M}_1) dv. \quad (4.127)$$

By following the same procedure as for the electric current case, we can derive the excitation coefficients of the n th waveguide mode as

$$A_n^+ = \frac{1}{P_n} \int_V \bar{H}_n^- \cdot \bar{M} dv = \frac{1}{P_n} \int_V (-\bar{h}_n + \hat{z}h_{zn}) \cdot \bar{M} e^{j\beta_n z} dv, \quad (4.128)$$

$$A_n^- = \frac{1}{P_n} \int_V \bar{H}_n^+ \cdot \bar{M} dv = \frac{1}{P_n} \int_V (\bar{h}_n + \hat{z}h_{zn}) \cdot \bar{M} e^{-j\beta_n z} dv, \quad (4.129)$$

where P_n is defined in (4.125).

4.8

EXCITATION OF WAVEGUIDES—APERTURE COUPLING

Besides the probe and loop feeds of the previous section, waveguides and other transmission lines can also be coupled through small apertures. One common application of such coupling is in directional couplers and power dividers, where power from one guide is coupled to another guide through small apertures in a common wall. Figure 4.29 shows a variety of waveguide and other transmission line configurations in which aperture coupling can be employed. We will first develop an intuitive explanation for the fact that a small aperture can be represented as an infinitesimal electric and/or magnetic dipole, then we will use the results of Section 4.7 to find the fields generated by these equivalent currents. Our analysis will be somewhat phenomenological [4, 10]; a more advanced theory of aperture coupling based on the equivalence theorem can be found in reference [11].

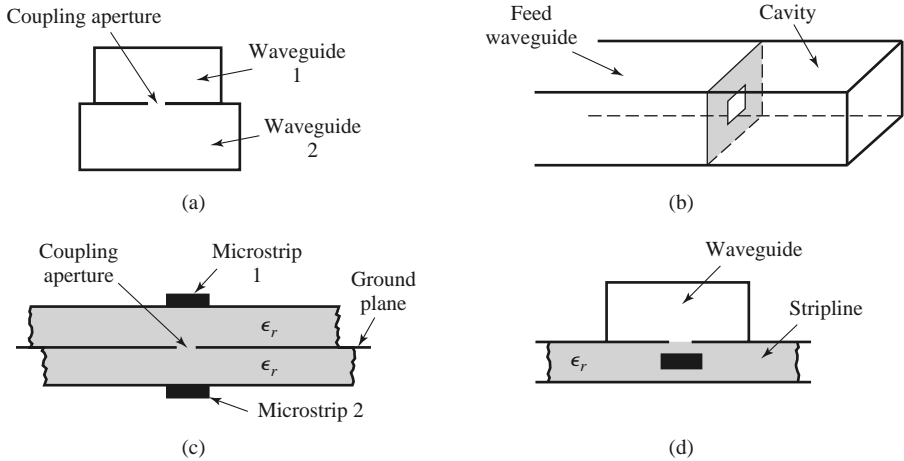


FIGURE 4.29 Various waveguide and other transmission line configurations using aperture coupling. (a) Coupling between two waveguides via an aperture in the common broad wall. (b) Coupling to a waveguide cavity via an aperture in a transverse wall. (c) Coupling between two microstrip lines via an aperture in the common ground plane. (d) Coupling from a waveguide to a stripline via an aperture.

Consider Figure 4.30a, which shows the normal electric field lines near a conducting wall (the tangential electric field is zero near the wall). If a small aperture is cut into the conductor, the electric field lines will fringe through and around the aperture as shown in Figure 4.30b. Now consider Figure 4.30c, which shows the fringing field lines around two infinitesimal electric polarization currents, \bar{P}_e , normal to a conducting wall (without

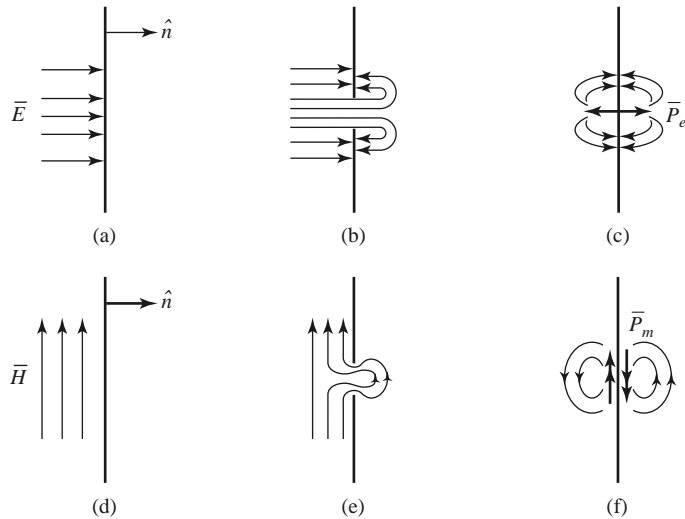


FIGURE 4.30 Illustrating the development of equivalent electric and magnetic polarization currents at an aperture in a conducting wall. (a) Normal electric field at a conducting wall. (b) Electric field lines around an aperture in a conducting wall. (c) Electric field lines around electric polarization currents normal to a conducting wall. (d) Magnetic field lines near a conducting wall. (e) Magnetic field lines near an aperture in a conducting wall. (f) Magnetic field lines near magnetic polarization currents parallel to a conducting wall.

an aperture). The similarity of the field lines of Figures 4.30c and 4.30b suggests that an aperture excited by a normal electric field can be represented by two oppositely directed infinitesimal electric polarization currents, \bar{P}_e , normal to the closed conducting wall. The strength of this polarization current is proportional to the normal electric field; thus,

$$\bar{P}_e = \epsilon_0 \alpha_e \hat{n} E_n \delta(x - x_0) \delta(y - y_0) \delta(z - z_0), \quad (4.130)$$

where the proportionality constant α_e is defined as the *electric polarizability* of the aperture, and (x_0, y_0, z_0) are the coordinates of the center of the aperture.

Similarly, Figure 4.30e shows the fringing of tangential magnetic field lines (the normal magnetic field is zero at the conductor) near a small aperture. Because these field lines are similar to those produced by two magnetic polarization currents located parallel to the conducting wall (as shown in Figure 4.30f), we can conclude that the aperture can be replaced by two oppositely directed infinitesimal polarization currents, \bar{P}_m , where

$$\bar{P}_m = -\alpha_m \bar{H}_t \delta(x - x_0) \delta(y - y_0) \delta(z - z_0). \quad (4.131)$$

In (4.131), α_m is defined as the *magnetic polarizability* of the aperture.

The electric and magnetic polarizabilities are constants that depend on the size and shape of the aperture and have been derived for a variety of simple shapes [3, 10, 11]. The polarizabilities for circular and rectangular apertures, which are probably the most commonly used shapes, are given in Table 4.3.

We now show that the electric and magnetic polarization currents, \bar{P}_e and \bar{P}_m , can be related to electric and magnetic current sources, \bar{J} and \bar{M} , respectively. From Maxwell's equations (1.27a) and (1.27b) we have

$$\nabla \times \bar{E} = -j\omega\mu\bar{H} - \bar{M}, \quad (4.132a)$$

$$\nabla \times \bar{H} = j\omega\epsilon\bar{E} + \bar{J}. \quad (4.132b)$$

Then using (1.15) and (1.23), which define \bar{P}_e and \bar{P}_m , we obtain

$$\nabla \times \bar{E} = -j\omega\mu_0\bar{H} - j\omega\mu_0\bar{P}_m - \bar{M}, \quad (4.133a)$$

$$\nabla \times \bar{H} = j\omega\epsilon_0\bar{E} + j\omega\bar{P}_e + \bar{J}. \quad (4.133b)$$

Thus, since \bar{M} has the same role in these equations as $j\omega\mu_0\bar{P}_m$, and \bar{J} has the same role as $j\omega\bar{P}_e$, we can define equivalent currents as

$$\bar{J} = j\omega\bar{P}_e, \quad (4.134a)$$

$$\bar{M} = j\omega\mu_0\bar{P}_m. \quad (4.134b)$$

These results allow us to use the formulas of (4.124), (4.126), (4.128), and (4.129) to compute the fields from these currents.

TABLE 4.3 Electric and Magnetic Polarizations

| Aperture Shape | α_e | α_m |
|--|---------------------------|---------------------------|
| Round hole | $\frac{2r_0^3}{3}$ | $\frac{4r_0^3}{3}$ |
| Rectangular slot (\bar{H} across slot) | $\frac{\pi \ell d^2}{16}$ | $\frac{\pi \ell d^2}{16}$ |

The above theory is approximate because of various assumptions involved in the evaluation of the polarizabilities, but generally it gives reasonable results for apertures that are small (where the term *small* implies small relative to an electrical wavelength), and not located too close to edges or corners of the guide. In addition, it is important to realize that the equivalent dipoles given by (4.130) and (4.131) radiate in the presence of the conducting wall to give the fields transmitted through the aperture. The fields on the input side of the conducting wall are also affected by the presence of the aperture, and this effect is accounted for by the equivalent dipoles on the incident side of the conductor (which are the negative of those on the output side). In this way, continuity of tangential fields is preserved across the aperture. In both cases, the presence of the (closed) conducting wall can be accounted for by using image theory to remove the wall and double the strength of the dipoles. These details will be clarified by applying this theory to apertures in transverse and broad walls of waveguides.

Coupling Through an Aperture in a Transverse Waveguide Wall

Consider a small circular aperture centered in the transverse wall of a waveguide, as shown in Figure 4.31a. Assume that only the TE₁₀ mode propagates in the guide, and is incident on the transverse wall from $z < 0$. Then, if the aperture is assumed to be closed, as in Figure 4.31b, the standing wave fields in the region $z < 0$ can be written as

$$E_y = A(e^{-j\beta z} - e^{j\beta z}) \sin \frac{\pi x}{a}, \quad (4.135a)$$

$$H_x = \frac{-A}{Z_{10}}(e^{-j\beta z} + e^{j\beta z}) \sin \frac{\pi x}{a}, \quad (4.135b)$$

where β and Z_{10} are the propagation constant and wave impedance of the TE₁₀ mode. From (4.130) and (4.131) we can determine the equivalent electric and magnetic polarization currents from the above fields as

$$\bar{P}_e = \hat{z}\epsilon_0\alpha_e E_z \delta\left(x - \frac{a}{2}\right) \delta\left(y - \frac{b}{2}\right) \delta(z) = 0, \quad (4.136a)$$

$$\begin{aligned} \bar{P}_m &= -\hat{x}\alpha_m H_x \delta\left(x - \frac{a}{2}\right) \delta\left(y - \frac{b}{2}\right) \delta(z) \\ &= \hat{x} \frac{2A\alpha_m}{Z_{10}} \delta\left(x - \frac{a}{2}\right) \delta\left(y - \frac{b}{2}\right) \delta(z), \end{aligned} \quad (4.136b)$$

since $E_z = 0$ for a TE mode. Now, by (4.134b), the magnetic polarization current \bar{P}_m is equivalent to the magnetic current density

$$\bar{M} = j\omega\mu_0\bar{P}_m = \hat{x} \frac{2j\omega\mu_0 A\alpha_m}{Z_{10}} \delta\left(x - \frac{a}{2}\right) \delta\left(y - \frac{b}{2}\right) \delta(z). \quad (4.137)$$

As shown in Figure 4.31d, the fields scattered by the aperture are considered as being produced by the equivalent currents \bar{P}_m and $-\bar{P}_m$ on either side of the closed wall. The presence of the conducting wall is easily accounted for using image theory, which has the effect of doubling the dipole strengths and removing the wall, as depicted in Figure 4.31e (for $z < 0$) and Figure 4.31f (for $z > 0$). Thus the coefficients of the transmitted and reflected waves caused by the equivalent aperture currents can be found by using (4.137) in (4.128) and (4.129) to give

$$A_{10}^+ = \frac{-1}{P_{10}} \int \bar{h}_{10} \cdot (2j\omega\mu_0\bar{P}_m) dv = \frac{4jA\omega\mu_0\alpha_m}{abZ_{10}} = \frac{4jA\beta\alpha_m}{ab}, \quad (4.138a)$$

$$A_{10}^- = \frac{-1}{P_{10}} \int \bar{h}_{10} \cdot (-2j\omega\mu_0\bar{P}_m) dv = \frac{4jA\omega\mu_0\alpha_m}{abZ_{10}} = \frac{4jA\beta\alpha_m}{ab}, \quad (4.138b)$$

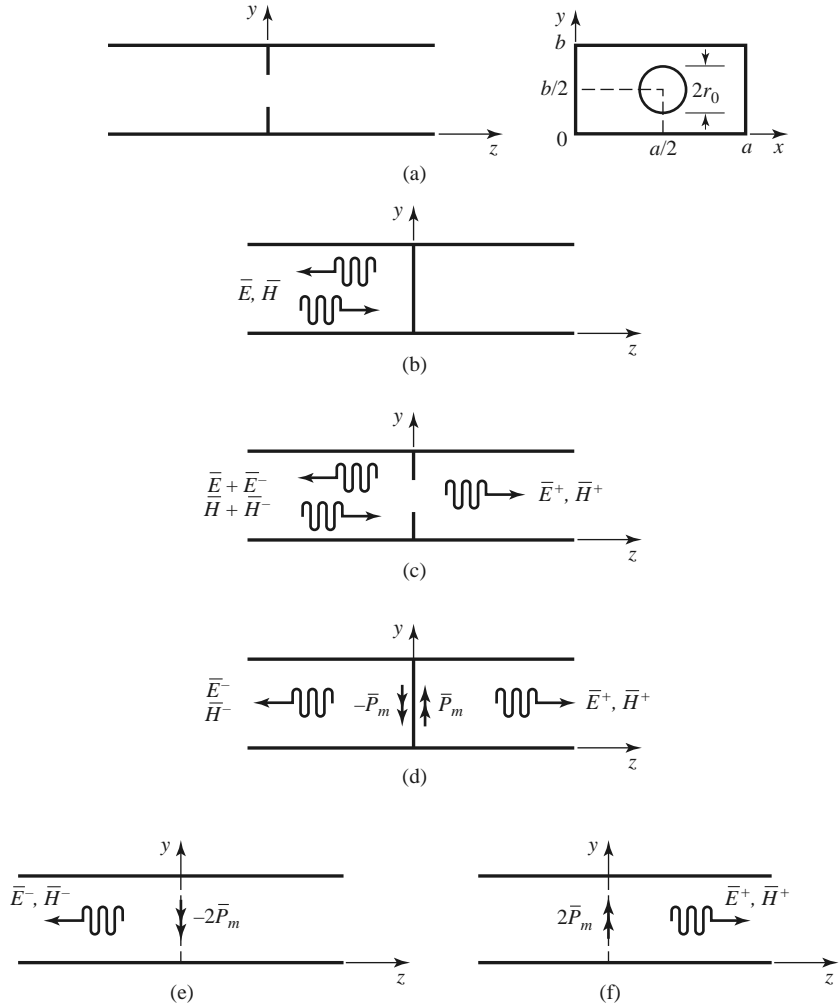


FIGURE 4.31 Applying small-hole coupling theory and image theory to the problem of an aperture in the transverse wall of a waveguide. (a) Geometry of a circular aperture in the transverse wall of a waveguide. (b) Fields with aperture closed. (c) Fields with aperture open. (d) Fields with aperture closed and replaced with equivalent dipoles. (e) Fields radiated by equivalent dipoles for $z < 0$; wall removed by image theory. (f) Fields radiated by equivalent dipoles for $z > 0$; wall removed by image theory.

since $\bar{h}_{10} = (-\hat{x}/Z_{10}) \sin(\pi x/a)$, and $P_{10} = ab/Z_{10}$. The magnetic polarizability α_m is given in Table 4.3. The complete fields can now be written as

$$E_y = [Ae^{-j\beta z} + (A_{10}^- - A)e^{j\beta z}] \sin \frac{\pi x}{a}, \quad \text{for } z < 0, \quad (4.139a)$$

$$H_x = \frac{1}{Z_{10}} [-Ae^{-j\beta z} + (A_{10}^- - A)e^{j\beta z}] \sin \frac{\pi x}{a}, \quad \text{for } z < 0, \quad (4.139b)$$

and

$$E_y = A_{10}^+ e^{-j\beta z} \sin \frac{\pi x}{a}, \quad \text{for } z > 0, \quad (4.140a)$$

$$H_x = \frac{-A_{10}^+}{Z_{10}} e^{-j\beta z} \sin \frac{\pi x}{a}, \quad \text{for } z > 0. \quad (4.140b)$$

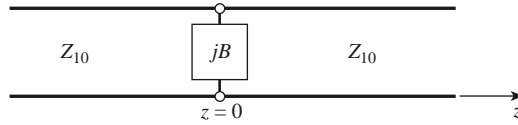


FIGURE 4.32 Equivalent circuit of the aperture in a transverse waveguide wall.

Then the reflection and transmission coefficients can be found as

$$\Gamma = \frac{A_{10}^- - A}{A} = \frac{4j\beta\alpha_m}{ab} - 1, \quad (4.141a)$$

$$T = \frac{A_{10}^+}{A} = \frac{4j\beta\alpha_m}{ab}, \quad (4.141b)$$

since $Z_{10} = k_0\eta_0/\beta$. Note that $|\Gamma| > 1$; this physically unrealizable result (for a passive network) is an artifact of the approximations used in the above theory. An equivalent circuit for this problem can be obtained by comparing the reflection coefficient of (4.141a) with that of the transmission line with a normalized shunt susceptance, jB , shown in Figure 4.32. The reflection coefficient seen looking into this line is

$$\Gamma = \frac{1 - y_{in}}{1 + y_{in}} = \frac{1 - (1 + jB)}{1 + (1 + jB)} = \frac{-jB}{2 + jB}.$$

If the shunt susceptance is very large (low impedance), Γ can be approximated as

$$\Gamma = \frac{-1}{1 + (2/jB)} \simeq -1 - j\frac{2}{B}.$$

Comparison with (4.141a) suggests that the aperture is equivalent to a normalized inductive susceptance,

$$B = \frac{-ab}{2\beta\alpha_m}.$$

Coupling Through an Aperture in the Broad Wall of a Waveguide

Another common configuration for aperture coupling is shown in Figure 4.33, where two parallel waveguides share a common broad wall and are coupled with a small centered aperture. We will assume a TE_{10} mode incident from $z < 0$ in the lower guide (guide 1),

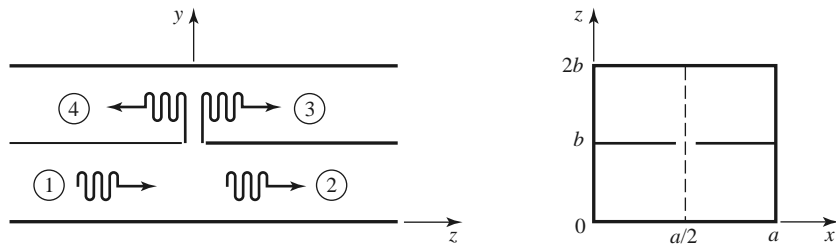


FIGURE 4.33 Two parallel waveguides coupled through an aperture in a common broad wall.

and compute the fields coupled to the upper guide. The incident fields can be written as

$$E_y = A \sin \frac{\pi x}{a} e^{-j\beta z}, \quad (4.142a)$$

$$H_x = \frac{-A}{Z_{10}} \sin \frac{\pi x}{a} e^{-j\beta z}. \quad (4.142b)$$

The excitation field at the center of the aperture at $(x = a/2, y = b, z = 0)$ is

$$E_y = A, \quad (4.143a)$$

$$H_x = \frac{-A}{Z_{10}}. \quad (4.143b)$$

(If the aperture were not centered at $x = a/2$, the H_z field would be nonzero and would have to be included.)

From (4.130), (4.131), and (4.134), the equivalent electric and magnetic dipoles for coupling to the fields in the upper guide are

$$J_y = j\omega\epsilon_0\alpha_e A \delta\left(x - \frac{a}{2}\right) \delta(y - b) \delta(z), \quad (4.144a)$$

$$M_x = \frac{j\omega\mu_0\alpha_m A}{Z_{10}} \delta\left(x - \frac{a}{2}\right) \delta(y - b) \delta(z). \quad (4.144b)$$

Note that in this case we have excited both an electric and a magnetic dipole. Let the fields in the upper guide be expressed as

$$E_y^- = A^- \sin \frac{\pi x}{a} e^{+j\beta z} \quad \text{for } z < 0, \quad (4.145a)$$

$$H_x^- = \frac{A^-}{Z_{10}} \sin \frac{\pi x}{a} e^{+j\beta z} \quad \text{for } z < 0, \quad (4.145b)$$

$$E_y^+ = A^+ \sin \frac{\pi x}{a} e^{-j\beta z} \quad \text{for } z > 0, \quad (4.146a)$$

$$H_x^+ = \frac{-A^+}{Z_{10}} \sin \frac{\pi x}{a} e^{-j\beta z} \quad \text{for } z > 0, \quad (4.146b)$$

where A^+ , A^- are the unknown amplitudes of the forward and backward traveling waves in the upper guide, respectively.

By superposition, the total fields in the upper guide due to the electric and magnetic currents of (4.144) can be found from (4.124) and (4.128) for the forward wave as

$$A^+ = \frac{-1}{P_{10}} \int_V (E_y^- J_y - H_x^- M_x) dv = \frac{-j\omega A}{P_{10}} \left(\epsilon_0 \alpha_e - \frac{\mu_0 \alpha_m}{Z_{10}^2} \right), \quad (4.147a)$$

and from (4.126) and (4.129) for the backward wave as

$$A^- = \frac{-1}{P_{10}} \int_V (E_y^+ J_y - H_x^+ M_x) dv = \frac{-j\omega A}{P_{10}} \left(\epsilon_0 \alpha_e + \frac{\mu_0 \alpha_m}{Z_{10}^2} \right), \quad (4.147b)$$

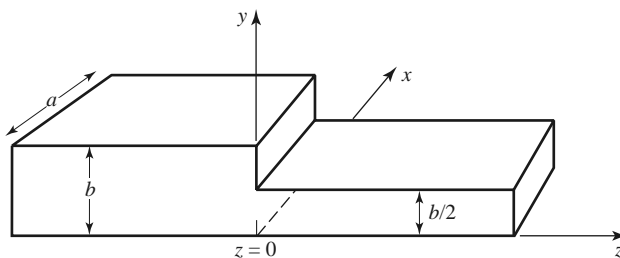
where $P_{10} = ab/Z_{10}$. Note that the electric dipole excites the same fields in both directions, but the magnetic dipole excites oppositely polarized fields in the forward and backward directions.

REFERENCES

- [1] S. Ramo, T. R. Whinnery, and T. van Duzer, *Fields and Waves in Communication Electronics*, John Wiley & Sons, New York, 1965.
- [2] A. A. Oliner, "Historical Perspectives on Microwave Field Theory," *IEEE Transactions on Microwave Theory and Techniques*, vol. MTT-32, pp. 1022–1045, September 1984.
- [3] C. G. Montgomery, R. H. Dicke, and E. M. Purcell, eds., *Principles of Microwave Circuits*, MIT Radiation Laboratory Series, Vol. 8, McGraw-Hill, New York, 1948.
- [4] R. E. Collin, *Foundations for Microwave Engineering*, 2nd edition, McGraw-Hill, New York, 1992.
- [5] J. Rahola, "Power Waves and Conjugate Matching," *IEEE Transactions on Circuits and Systems*, vol. 55, pp. 92–96, January 2008.
- [6] J. S. Wright, O. P. Jain, W. J. Chudobiak, and V. Makios, "Equivalent Circuits of Microstrip Impedance Discontinuities and Launchers," *IEEE Transactions on Microwave Theory and Techniques*, vol. MTT-22, pp. 48–52, January 1974.
- [7] G. F. Engen and C. A. Hoer, "Thru-Reflect-Line: An Improved Technique for Calibrating the Dual Six-Port Automatic Network Analyzer," *IEEE Transactions on Microwave Theory and Techniques*, vol. MTT-27, pp. 987–998, December 1979.
- [8] N. Marcuvitz, ed., *Waveguide Handbook*, MIT Radiation Laboratory Series, Vol. 10, McGraw-Hill, New York, 1948.
- [9] K. C. Gupta, R. Garg, and I. J. Bahl, *Microstrip Lines and Slotlines*, Artech House, Dedham, Mass., 1979.
- [10] G. Matthaei, L. Young, and E. M. T. Jones, *Microwave Filters, Impedance-Matching Networks, and Coupling Structures*, Artech House, Dedham, Mass., 1980, Chapter 5.
- [11] R. E. Collin, *Field Theory of Guided Waves*, McGraw-Hill, New York, 1960.

PROBLEMS

- 4.1 Consider the reflection of a TE_{10} mode, incident from $z < 0$, at a step change in the height of a rectangular waveguide, as shown below. Show that if the method of Example 4.2 is used, the result $\Gamma = 0$ is obtained. Do you think this is the correct solution? Why? (This problem shows that the one-mode impedance viewpoint does not always provide a correct analysis.)

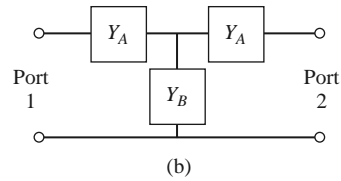
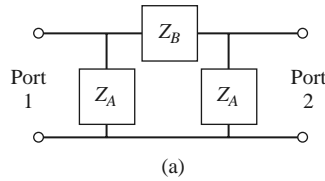


- 4.2 Consider a series RLC circuit with a current I . Calculate the power lost and the stored electric and magnetic energies, and show that the input impedance can be expressed as in (4.17).
- 4.3 Show that the input impedance Z of a parallel RLC circuit satisfies the condition that $Z(-\omega) = Z^*(\omega)$.
- 4.4 A two-port network is driven at both ports such that the port voltages and currents have the following values ($Z_0 = 50 \Omega$):

$$\begin{aligned} V_1 &= 10\angle 90^\circ, & I_1 &= 0.2\angle 90^\circ, \\ V_2 &= 8\angle 0^\circ, & I_2 &= 0.16\angle -90^\circ. \end{aligned}$$

Determine the input impedance seen at each port, and find the incident and reflected voltages at each port.

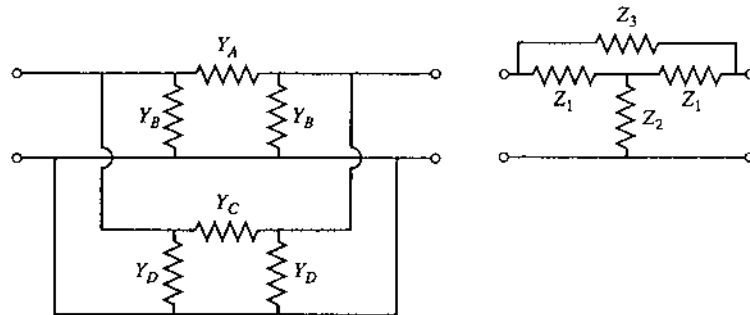
- 4.5 Show that the admittance matrix of a lossless N -port network has purely imaginary elements.
- 4.6 Does a nonreciprocal lossless network always have a purely imaginary impedance matrix?
- 4.7 Derive the $[Z]$ and $[Y]$ matrices for the two-port networks shown in the figure below.



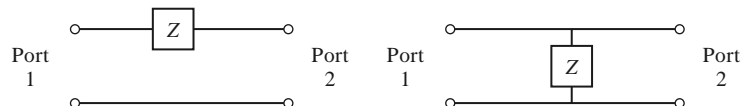
- 4.8 Consider a two-port network, and let $Z_{SC}^{(1)}$, $Z_{SC}^{(2)}$, $Z_{OC}^{(1)}$, and $Z_{OC}^{(2)}$ be the input impedance seen when port 2 is short-circuited, when port 1 is short-circuited, when port 2 is open-circuited, and when port 1 is open-circuited, respectively. Show that the impedance matrix elements are given by

$$Z_{11} = Z_{OC}^{(1)}, \quad Z_{22} = Z_{OC}^{(2)}, \quad Z_{12}^2 = Z_{21}^2 = (Z_{OC}^{(1)} - Z_{SC}^{(1)}) Z_{OC}^{(2)}.$$

- 4.9 Find the impedance parameters of a section of transmission line with length ℓ , characteristic impedance Z_0 , and propagation constant β .
- 4.10 Show that the admittance matrix of the two parallel-connected two-port π networks shown below can be found by adding the admittance matrices of the individual two-ports. Apply this result to find the admittance matrix of the bridged-T circuit shown. What is the corresponding result for the impedance matrix of two series-connected T-networks?



- 4.11 Find the scattering parameters for the series and shunt loads shown below. Show that $S_{12} = 1 - S_{11}$ for the series case, and that $S_{12} = 1 + S_{11}$ for the shunt case. Assume a characteristic impedance Z_0 .



- 4.12 Consider two two-port networks with individual scattering matrices $[S^A]$ and $[S^B]$. Show that the overall S_{21} parameter of the cascade of these networks is given by

$$S_{21} = \frac{S_{21}^A S_{21}^B}{1 - S_{22}^A S_{11}^B}.$$

- 4.13 Consider a lossless two-port network. (a) If the network is reciprocal, show that $|S_{21}|^2 = 1 - |S_{11}|^2$. (b) If the network is nonreciprocal, show that it is impossible to have unidirectional transmission, where $S_{12} = 0$ and $S_{21} \neq 0$.

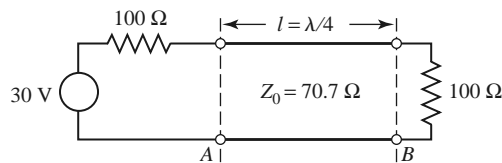
- 4.14** A four-port network has the scattering matrix shown as follows. (a) Is this network lossless? (b) Is this network reciprocal? (c) What is the return loss at port 1 when all other ports are terminated with matched loads? (d) What is the insertion loss and phase delay between ports 2 and 4 when all other ports are terminated with matched loads? (e) What is the reflection coefficient seen at port 1 if a short circuit is placed at the terminal plane of port 3 and all other ports are terminated with matched loads?

$$[S] = \begin{bmatrix} 0.178\angle 90^\circ & 0.6\angle 45^\circ & 0.4\angle 45^\circ & 0 \\ 0.6\angle 45^\circ & 0 & 0 & 0.3\angle -45^\circ \\ 0.4\angle 45^\circ & 0 & 0 & 0.5\angle -45^\circ \\ 0 & 0.3\angle -45^\circ & 0.5\angle -45^\circ & 0 \end{bmatrix}.$$

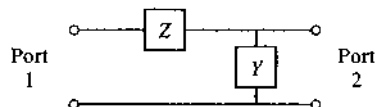
- 4.15** Show that it is impossible to construct a three-port network that is lossless, reciprocal, and matched at all ports. Is it possible to construct a nonreciprocal three-port network that is lossless and matched at all ports?
- 4.16** Prove the following *decoupling theorem*: For any lossless reciprocal three-port network, one port (say port 3) can be terminated in a reactance so that the other two ports (say ports 1 and 2) are decoupled (no power flow from port 1 to port 2, or from port 2 to port 1).
- 4.17** A certain three-port network is lossless and reciprocal, and has $S_{13} = S_{23}$ and $S_{11} = S_{22}$. Show that if port 2 is terminated with a matched load, then port 1 can be matched by placing an appropriate reactance at port 3.
- 4.18** A four-port network has the scattering matrix shown as follows. If ports 3 and 4 are connected with a lossless matched transmission line with an electrical length of 45° , find the resulting insertion loss and phase delay between ports 1 and 2.

$$[S] = \begin{bmatrix} 0.2\angle 50^\circ & 0 & 0 & 0.4\angle -45^\circ \\ 0 & 0.6\angle 45^\circ & 0.7\angle -45^\circ & 0 \\ 0 & 0.7\angle -45^\circ & 0.6\angle 45^\circ & 0 \\ 0.4\angle -45^\circ & 0 & 0 & 0.5\angle 45^\circ \end{bmatrix}.$$

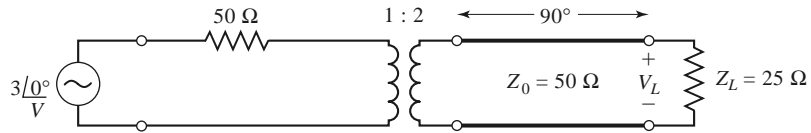
- 4.19** When normalized to a single characteristic impedance Z_0 , a certain two-port network has scattering parameters S_{ij} . Find the generalized scattering parameters, S_{ij}^p , in terms of the real reference impedances, R_{01} and R_{02} , at ports 1 and 2, respectively.
- 4.20** At reference plane A, for the circuit shown below, choose an appropriate reference impedance, find the power wave amplitudes, and compute the power delivered to the load. Repeat this procedure for reference plane B. Assume the transmission line is lossless.



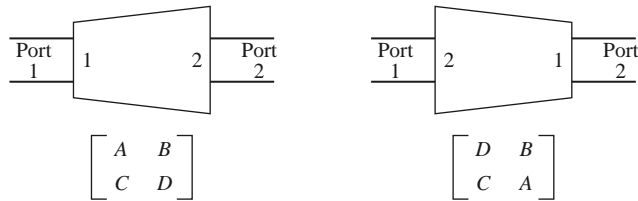
- 4.21** The $ABCD$ parameters of the first entry in Table 4.1 were derived in Example 4.6. Verify the $ABCD$ parameters for the second, third, and fourth entries.
- 4.22** Derive expressions that give the impedance parameters in terms of the $ABCD$ parameters.
- 4.23** Find the $ABCD$ matrix for the circuit shown below by direct calculation using the definition of the $ABCD$ matrix, and compare with the $ABCD$ matrix of the appropriate cascade of canonical circuits from Table 4.1.



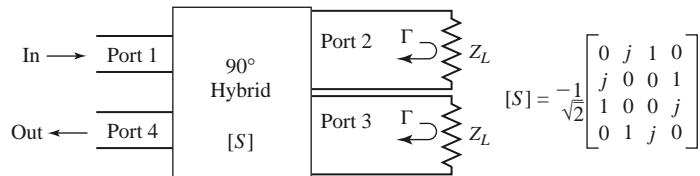
- 4.24 Use $ABCD$ matrices to find the voltage V_L across the load resistor in the circuit shown below.



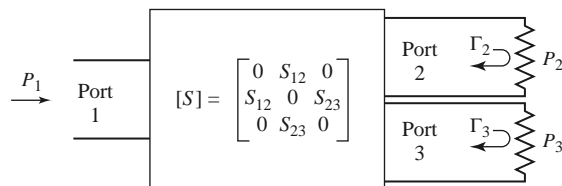
- 4.25 A reciprocal two-port network with its $ABCD$ matrix is shown below at left. Prove that the network with ports 1 and 2 in reversed positions has the $ABCD$ matrix shown below at right. Choose a simple asymmetrical network to demonstrate this result.



- 4.26 Derive the expressions for S parameters in terms of the $ABCD$ parameters, as given in Table 4.2.
- 4.27 As shown in the figure below, a variable attenuator can be implemented using a four-port 90° hybrid coupler by terminating ports 2 and 3 with equal but adjustable loads. (a) Using the given scattering matrix for the coupler, show that the transmission coefficient between the input (port 1) and the output (port 4) is given as $T = j\Gamma$, where Γ is the reflection coefficient of the mismatch at ports 2 and 3. Also show that the input port is matched for all values of Γ . (b) Plot the attenuation, in dB, from the input to the output as a function of Z_L/Z_0 , for $0 \leq Z_L/Z_0 \leq 10$ (let Z_L be real).



- 4.28 Use signal flow graphs to find the power ratios P_2/P_1 and P_3/P_1 for the mismatched three-port network shown in the accompanying figure.



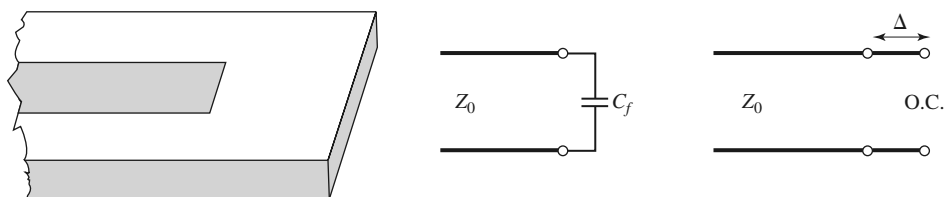
- 4.29 The $ABCD$ parameters are useful for treating cascades of two-port networks in terms of the total port voltages and currents, but it is also possible to use incident and reflected voltages to treat cascades. One way of doing this is with the *transfer*, or T -, parameters, defined as follows:

$$\begin{bmatrix} a_1 \\ b_1 \end{bmatrix} = \begin{bmatrix} T_{11} & T_{12} \\ T_{21} & T_{22} \end{bmatrix} \begin{bmatrix} b_2 \\ a_2 \end{bmatrix},$$

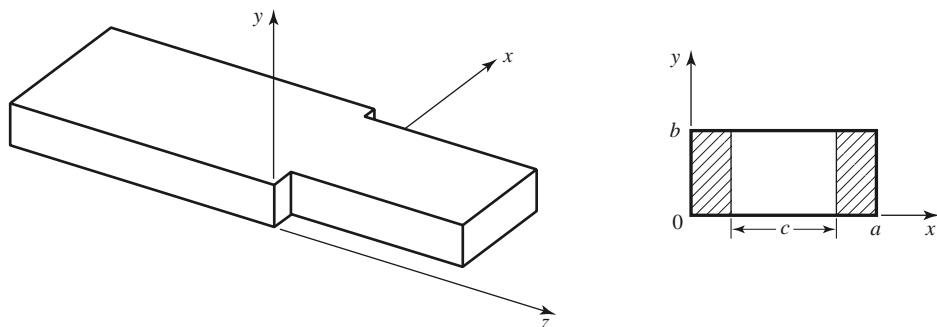
where a_1, b_1 and a_2, b_2 are the incident and reflected voltages at ports 1 and 2, respectively. Derive the T -parameters in terms of the scattering parameters of a two-port network. Show how the T -parameters can be used for a cascade of two two-port networks.

- 4.30** The end of an open-circuited microstrip line has fringing fields that can be modeled as a shunt capacitor, C_f , at the end of the line, as shown below. This capacitance can be replaced with an additional length, Δ , of microstrip line. Derive an expression for the length extension in terms of the fringing capacitance. Evaluate the length extension for a $50\ \Omega$ open-circuited microstrip line on a substrate with $d = 0.158\text{ cm}$ and $\epsilon_r = 2.2$ ($w = 0.487\text{ cm}$, $\epsilon_e = 1.894$), if the fringing capacitance is known to be $C_f = 0.075\text{ pF}$. Compare your result with the approximation given by Hammerstad and Bekkadal:

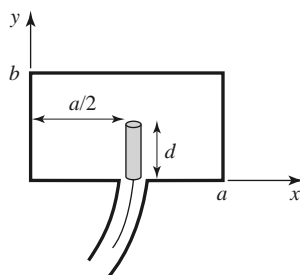
$$\Delta = 0.412d \left(\frac{\epsilon_e + 0.3}{\epsilon_e - 0.258} \right) \left(\frac{w + 0.262d}{w + 0.813d} \right).$$



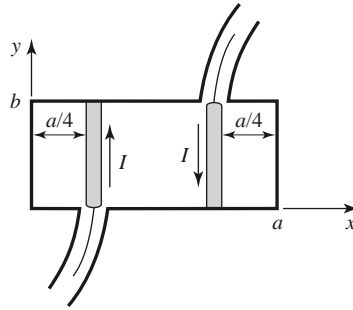
- 4.31** For the H -plane step analysis of Section 4.6, compute the complex power flow in the reflected modes in guide 1, and show that the reactive power is inductive.
- 4.32** Derive the modal analysis equations for the symmetric H -plane step shown below. (HINT: Because of symmetry, only the TE_{n0} modes for n odd will be excited.)



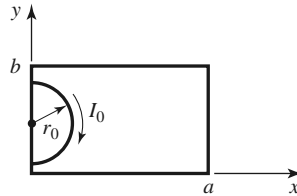
- 4.33** Find the transverse \vec{E} and \vec{H} fields excited by the current of (4.116) by postulating traveling TM_{mn} modes on either side of the source at $z = 0$ and applying the appropriate boundary conditions.
- 4.34** An infinitely long rectangular waveguide is fed with a probe of length d as shown below. The current on this probe can be approximated as $I(y) = I_0 \sin k(d - y)/\sin kd$. If the TE_{10} mode is the only propagating mode in the waveguide, compute the input resistance seen at the probe terminals.



- 4.35** Consider the infinitely long waveguide fed with two probes driven 180° out of phase, as shown below. What are the resulting excitation coefficients for the TE_{10} and TE_{20} modes? What other modes can be excited by this feeding arrangement?



- 4.36** Consider a small current loop on the sidewall of a rectangular waveguide, as shown below. Find the TE_{10} fields excited by this loop if the loop is of radius r_0 .



- 4.37** A rectangular waveguide is shorted at $z = 0$ and has an electric current sheet, J_{sy} , located at $z = d$, where

$$J_{sy} = \frac{2\pi A}{a} \sin \frac{\pi x}{a}$$

(see the accompanying figure). Find expressions for the fields generated by this current by assuming standing wave fields for $0 < z < d$, and traveling wave fields for $z > d$, and applying boundary conditions at $z = 0$ and $z = d$. Now solve the problem using image theory, by placing a current sheet $-J_{sy}$ at $z = -d$, and removing the shorting wall at $z = 0$. Use the results of Section 4.7 and superposition to find the fields radiated by these two currents, which should be the same as the first results for $z > 0$.

